THE ASTROPHYSICAL JOURNAL, 263:443–467, 1982 December 1

THE TROPOSPHERIC GAS COMPOSITION OF JUPITER'S NORTH EQUATORIAL BELT (NH_3, PH_3, CH_3D, GeH_4, H_2O) AND THE JOVIAN D/H ISOTOPIC RATIO

V. KUNDE, R. HANEL, AND W. MAGUIRE
NASA Goddard Space Flight Center
D. GAUTIER, J. P. BALUTEAU, AND A. MARTEN
Observatoire de Paris
AND
A. CHEDIN, N. HUSSON, AND N. SCOTT
Laboratoire de Meteorologie Dynamique du CNRS, Ecole Polytechnique
Received 1982 February 19; accepted 1982 May 18

ABSTRACT

The gas composition of the troposphere of Jupiter in the clearest regions of the North Equatorial Belt (NEB) was derived from the *Voyager 1* IRIS data. The infrared spectrum for this homogeneous "cloud-free" region was modeled to infer altitude profiles for NH_3, PH_3, CH_3D, GeH_4, and H_2O. The profiles for NH_3 and PH_3 were found to be depleted in the upper troposphere but otherwise in agreement with their solar values at the 1 bar level. The mole fraction for CH_3D was determined to be $3.5^{+1.0}_{-1.3} \times 10^{-7}$. The GeH_4 mole fraction of $7 \pm 2 \times 10^{-10}$ at the 2–5 bar level is a factor of 10 lower than the solar value. The H_2O mole fraction is $\sim 1 \times 10^{-6}$ at the 2.5 bar level and is increasing to $\sim 3 \times 10^{-5}$ at 4 bars where it is a factor of 30 lower than solar. Using IRIS inferred values for the mole fractions of CH_3D and CH_4 a value of $D/H = 3.6^{+1.0}_{-1.4} \times 10^{-5}$ is derived. Assuming this Jovian D/H ratio is representative of the protosolar nebula, and correcting for chemical galactic evolution, yields a value of $5.5\text{–}9.0 \times 10^{-5}$ for the primordial D/H ratio and an upper limit of $1.8\text{–}2.4 \times 10^{-31}$ g cm^{-3} for the present-day baryon density.

Subject headings: infrared: spectra — planets: abundances — planets: atmospheres — planets: Jupiter — planets: spectra

I. INTRODUCTION

Knowledge of the atmospheric composition and its vertical and horizontal variation is important for understanding the physical and chemical processes presently active on Jupiter. Information on the relative elemental abundances and their isotopic ratios, which may also be inferred from molecular abundances, help in a better understanding of the formation and evolution of Jupiter and the solar system as a whole. Because of the large mass and low exospheric temperatures Jupiter is believed to still have primordial composition. Comparison of Jovian abundances with corresponding solar values is thus equally important for theories of Jovian, solar, and solar system evolution. Analysis of the thermal emission spectrum allows detection and in some cases measurement of vertical distributions of several gases. This paper discusses the chemical composition and physical state of the Jovian atmosphere between 0.2 and 5 bars in the North Equatorial Belt.

In the last decade ground-based and airborne spectral measurements of the emitted infrared radiation have produced extensive information on the gaseous composition of the Jovian atmosphere (Encrenaz and Combes 1981; Larson 1977; Ridgway, Larson, and Fink 1976). The accuracy of these results, however, has often been limited by the lack of spatial resolution, and the ensuing complications in interpretation due to inhomogeneous cloud fields.

The *Voyager* IRIS (Infrared Interferometer Spectrometer and Radiometer) measurements cover the spectral range from 180 to 2500 cm^{-1} with 4.3 cm^{-1} resolution and offer several important improvements over previous ground-based and airborne data. First, a large number of spectra were obtained at various locations on the disk of the planet with a spatial resolution as high as 1° in Jovian latitude near closest approach. This high spatial resolution allows the separation of characteristic features; thus, it is possible to select spectra from belts where the influence of clouds is negligible and from zones where clouds are apparent. Second, the wide spectral range of the IRIS allows the retrieval of temperature structure and composition information simultaneously and within the same volume element, thus eliminating uncertainties due to temporal and spatial variations. Third, the wide spectral range allows also the simultaneous retrieval of the concentrations of several key atmospheric gases.

This paper is concerned with the gaseous composition of the lower atmosphere in the North Equatorial Belt (NEB). Clouds in the equatorial region have been studied by Marten *et al.* (1981). Section II describes the selection of the spectra. Section III discusses the radiative transfer

techniques used to obtain the thermal profile and the composition. Sections IV, V, and VI treat the analysis techniques and the results of the molecular composition study. Section VII discusses the D/H isotopic ratio, and finally § VIII presents conclusions.

II. OBSERVATIONS AND SELECTION CRITERIA

Approximately 25,000 Jovian spectra were acquired by the IRIS during the *Voyager 1* flyby for varying latitudes, emission angles, and local time (Hanel *et al.* 1979). Different locations on the planet show significant differences in their spectra. For this study the NEB has been chosen for analysis as it represents the most prominent, well defined cloud-free region at the time of the *Voyager 1* flyby (Terrile *et al.* 1979). Furthermore, many observational sequences were aimed at the NEB, thus providing an ample set of spectra. The signal-to-noise ratio (S/N) for an individual measurement varies across the spectrum, decreasing from ~ 200 at 200 cm^{-1} to about 5 at 2000 cm^{-1}. Because of the low signal-to-noise ratio at 2000 cm^{-1} it is necessary to average a number of individual spectra. The optimum number is a tradeoff between the desired signal-to-noise ratio and the required degree of atmospheric homogeneity in the ensemble. The selection criteria applied in this investigation are:

1. *Latitudinal extent.*—The ground-based maps of the Jovian disk at 2000 cm^{-1} show strong emission covering most of the NEB from approximately 8° to 13°N latitude (Terrile *et al.* 1979). Therefore the center point of the IRIS field of view (FOV) has been restricted to these latitudes.

2. *Spatial resolution.*—To assure that the projected field of view on Jupiter is less than the latitudinal extent of the NEB, only spectra obtained with a spatial resolution of less than 5° in latitude were accepted. All admitted spectra were recorded within ± 1 day of closest approach. The highest spatial resolution in the sample is 0°.8 in latitude.

3. *Emission angle.*—This angle has been arbitrarily chosen to be less than 30°, corresponding to an air mass of less than 1.15.

The above criteria define an ensemble of spectra for the NEB under near-vertical viewing conditions and with sufficient spatial resolution. However, considerable longitudinal atmospheric inhomogeneity can be noted in this ensemble, and it is necessary to define two additional criteria to assure selection of the clearest and most homogeneous cases. The continuum levels of the IRIS spectrum near 226 cm^{-1} and 2000 cm^{-1} are very sensitive indicators of the presence of haze and clouds at the 0.8 bar and 2–3 bar levels, respectively. The highest brightness temperatures correspond to the clearest conditions. Two other selection criteria are therefore added:

4. *226 cm^{-1} continuum.*—Only spectra with brightness temperatures higher than 149 K at 226 cm^{-1} have been selected, and,

5. *2000 cm^{-1} continuum.*—Only spectra with an average brightness temperature higher than 250 K averaged over 1950–2150 cm^{-1} were accepted.

Out of 25,207, only 51 spectra passed all five criteria. The average spectrum and the standard deviation (δT_{BB}) of this ensemble are shown in Figures 1 and 2. The average air mass factor for this ensemble is 1.04, corresponding to an equivalent emission angle of 15°.8. The signal-to-noise ratio for the average spectrum is ~ 1400 at 200 cm^{-1}, decreasing to ~ 35 at 2000 cm^{-1}. The standard deviations shown in Figures 1*b* and 2*b* are due mostly to longitudinal inhomogeneities in the troposphere of the NEB, the instrument noise being a factor of ~ 10 lower. In spite of this, the relatively small amplitude of the standard deviation indicates that the average spectrum represents a fairly homogeneous region.

The average spectrum shows the signatures of H_2, CH_4, C_2H_2, NH_3, PH_3, H_2O, GeH_4, and CH_3D. The spectrum divides naturally into two regimes: 180–1500 cm^{-1} (Fig. 1), which corresponds to thermal emission mostly from above the 1 bar level and 1800–2250 cm^{-1} (Fig. 2), which corresponds to emission mostly from below that level. The altitude from which the maximum contribution to the emission originates (unit optical depth) is illustrated in Figures 3 and 4. These 1/*e* levels have been computed with the help of the model atmosphere described in § III. It is evident from Figures 3 and 4 that the IRIS NEB spectrum contains information on the abundances of NH_3, PH_3, CH_3D, H_2O,

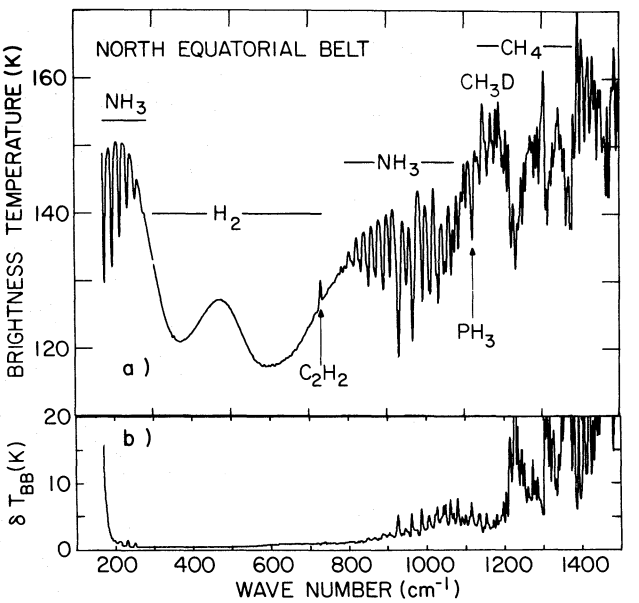

FIG. 1.—Observed thermal emission spectrum for the clearest region of the NEB between 180 and 1500 cm^{-1}. This spectrum is an average of 51 individual spectra. The spectral features observed for the gases H_2, NH_3, PH_3, and CH_3D are of tropospheric and C_2H_2 is of stratospheric origin. CH_4 is well mixed through both regions. The small standard deviation in brightness temperature, shown in the lower panel, indicates the average spectrum represents a very homogeneous region of the NEB.

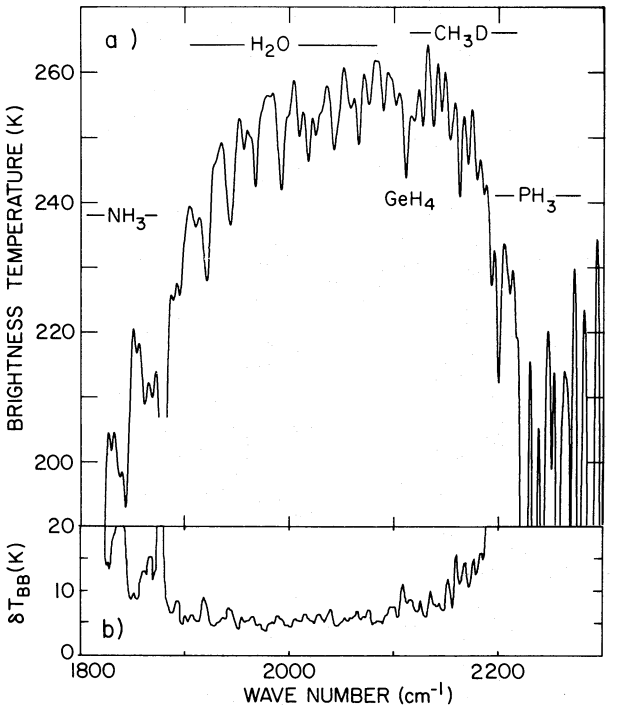

FIG. 2.—Observed thermal emission spectrum for the clearest region of the NEB between 1800 and 2250 cm^{-1}. This spectrum is an average of 51 individual spectra. The spectral features observed for the gases NH_3, H_2O, GeH_4, CH_3D, and PH_3 originate at 1–5 bar. The small standard deviation in brightness temperature, shown in the lower panel, indicates the average spectrum represents a very homogeneous region of the NEB.

and GeH_4 between approximately 0.2 and 5 bars. The information on the relevant altitudes will be discussed for each gas individually after presentation of the appropriate radiative transfer equation and the analysis procedures.

III. RADIATIVE TRANSFER ASPECTS

Retrieval of the thermal structure is the first step in the abundance determination. Vertical temperature profiles have been inferred from the IRIS spectrum by inversion of the radiative transfer equation, using measurements at selected wave numbers within the $S(0)$ and $S(1)$ lines of H_2 (285–610 cm^{-1}), and in the core of the ν_4 band of CH_4 (1250–1350 cm^{-1}). A CH_4 mole fraction of 1.75×10^{-3} was assumed, which is 2.07 times the solar value (Gautier *et al.* 1982). Preliminary Jovian temperature profiles from *Voyager* IRIS data have been presented by Hanel *et al.* (1979), with inversion techniques and typical weighting functions illustrated by Conrath and Gautier (1979), Gautier, Lacombe, and Revah (1977), and Conrath and Revah (1972). Figure 5 shows the profile retrieved from the spectrum of Figure 1. Information on the thermal structure is limited to the pressure range from 0.001 to 0.8 bar. To derive temperatures down to 5 bars, which is necessary for analysis of the 2000 cm^{-1} window measurements, the IRIS profile has been extrapolated to deeper levels with an adiabatic lapse rate calculated for a hydrogen mole fraction of 0.90 (Gautier *et al.* 1981) and taking into account the variation of specific heat with temperature. The dashed curve in Figure 5 represents this extrapolation.

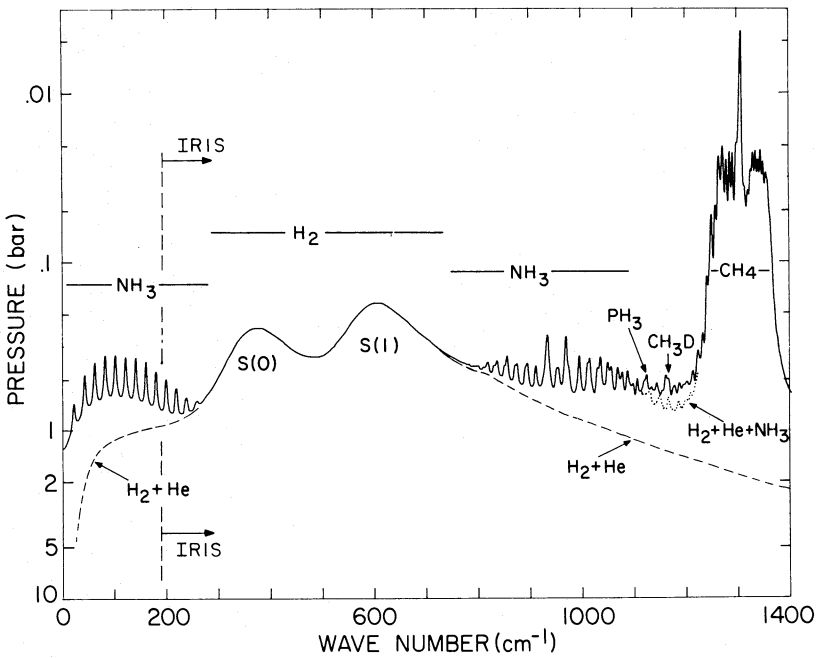

FIG. 3.—Atmospheric pressure levels where the optical depth equals unity for the 0–1400 cm^{-1} region. The maximum contribution to the emergent radiation originates from this level.

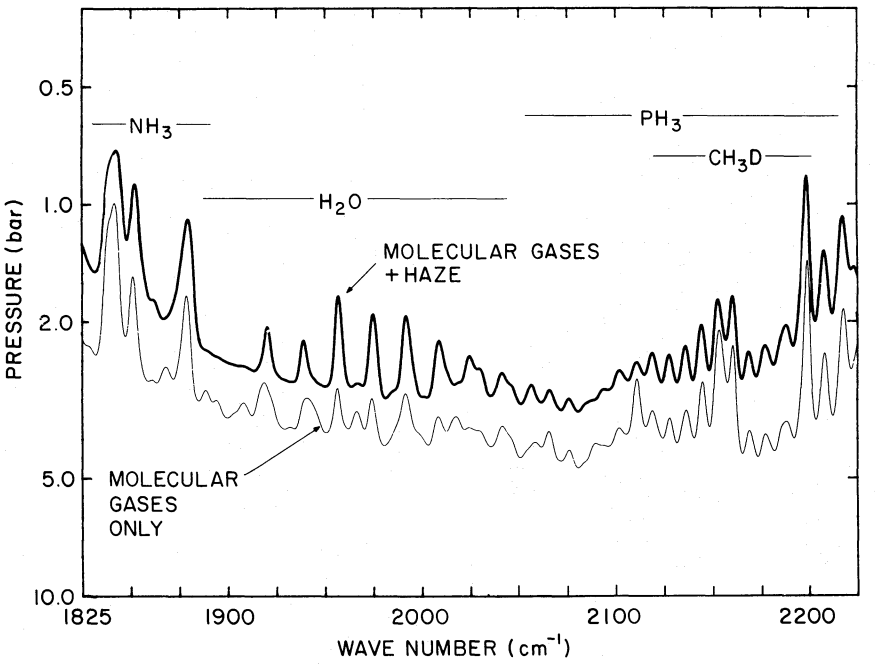

FIG. 4.—Same as Fig. 3, except for 1825–2225 cm^{-1} region

After the temperature profile is established, the gas abundances may be determined. A "best fit" approach has been used for the retrieval of vertical distributions, except for NH_3 where the inversion method of Smith (1970) was used. In the "best fit" approach spectra are synthesized using the radiative transfer equation, the derived temperature profile and assumed vertical distributions of the absorbing gases. The gas distributions are then iterated until the synthetic and observed spectra agree within error limits.

The monochromatic radiance for vertical viewing of a planetary atmosphere in local thermodynamic equilibrium is

$$I(\nu) = \int B(\nu, T) d\tau(\nu, P) , \qquad (1)$$

where the integration is from the top of the atmosphere down to a lower boundary; B is the Planck function at temperature T and wave number ν. The monochromatic slant path transmittance through an inhomogeneous medium is

$$\tau(\nu, P) = \exp\left[-(L_g + L_h)\right] . \qquad (2)$$

The optical depth, L_g, of a mixture of gases is

$$L_g = \int \sum_l C k^l(\nu, P, T)(q^l/g) dP , \qquad (3)$$

with C a constant; P, pressure; g, gravity; k^l, the molecular absorption coefficient; q_l, the mole fraction for the lth gas which is defined by

$$q_l = \frac{P_l}{P_{H_2} + P_{He} + \cdots} ; \qquad (4)$$

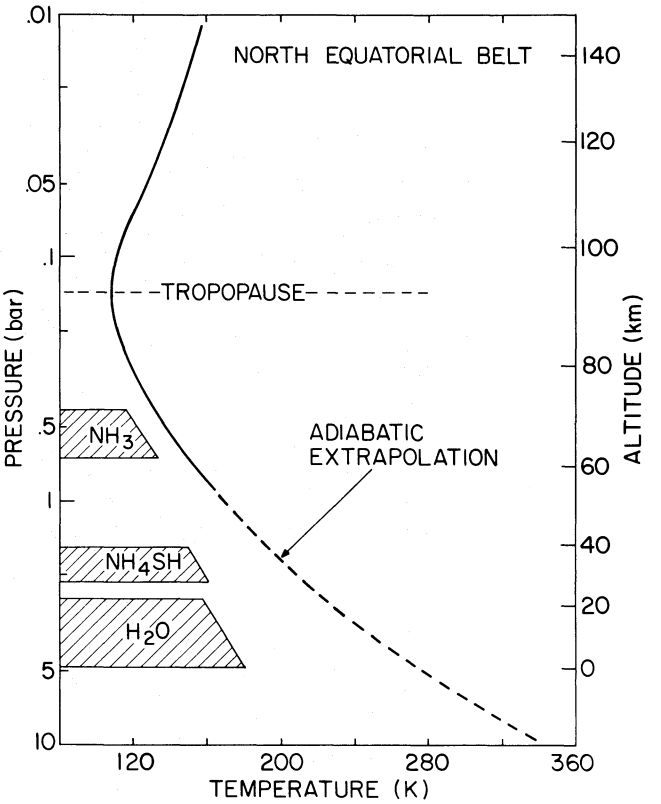

FIG. 5.—Temperature structure for the NEB. The solid line represents the temperature profile obtained by inversion of the NEB spectral radiances within the $S(0)$ and $S(1)$ H_2 lines and the 1306 cm^{-1} band of CH_4. The dashed line is an extrapolation from 0.8 bar to deeper levels along a $\sim$2.0 K km^{-1} adiabat. The theoretical cloud layers of Weidenschilling and Lewis 1973 are indicated schematically on the left.

and P_l, the partial pressure of the lth gas. The haze optical depth is

$$L_h = \int \sigma N(z) dz = \sigma N(z_0) e^{-\left[\frac{(z - z_0)}{H_h}\right]} \quad (5)$$

where σ is the extinction cross section; $N(z)$, the number density at altitude z; z_0, the altitude at the base of haze layer; and H_h, the haze scale height. Only the absorption cross section of the haze is included in this formulation, with scattering effects neglected. In the 180–1500 cm^{-1} range, the effect of haze is negligible for the NEB (Marten *et al.* 1981). Thus, the haze has been included only in the analysis of the 1850–2250 cm^{-1} region. The computed monochromatic radiances are convolved with the IRIS instrument function to obtain synthetic spectra with a resolution compatible with the measured spectra. The radiance and transmittance calculations rely on a multilayer model of the atmosphere and on a direct spectral integration procedure (Scott and Chedin 1981; Kunde and Maguire 1974; Scott 1973) for absorption by H_2, CH_4, NH_3, PH_3, CH_3D, H_2O, and GeH_4. The distributions for NH_3 and H_2O were also required not to exceed saturation. The molecular parameters used have been assembled into a line atlas as detailed in the Appendix.

The shapes of absorption lines were described by the Voigt line shape for pressures less than 0.1 bar and by the collisionally-broadened Lorentz shape for pressures greater than 0.1 bar. It is generally agreed that for pressures larger than 0.1 bar the Lorentz profile is appropriate for the cores of the lines, but it is uncertain how far into the wings it is valid. Theoretical and experimental studies indicate an exponential modification to the Lorentz line shape in the far wings of absorption bands for CO_2 and other species (Birnbaum 1979; Winters, Silverman, and Benedict 1964). Such a sub-Lorentzian behavior dramatically affects calculations of the continuum opacity in atmospheric "windows." The far wing effect on the continuum regions in the IRIS spectrum has been discussed by Kunde (1982). In the absence of information on the real behavior of the far wings of absorption lines considered here, we have simulated the sub-Lorentzian behavior by limiting the calculation of the Lorentz profile to a certain spectral distance from the center of each line. In the 180–1500 cm^{-1} range, we have limited calculations to 1200 half-widths from the line center at each atmospheric level (corresponding to 120 cm^{-1} for $\alpha_0 = 0.075$ cm^{-1} at 1 bar and 170 K), although tests were made for other values of the cut-off. In the 1800–2250 cm^{-1} range, calculations were limited to 250 cm^{-1} from the line center at each atmospheric level. The coefficient of 0.5 used for the temperature dependence of the line half-widths is in accord with kinetic theory.

IV. GAS DISTRIBUTIONS FROM THE 180–1300 cm^{-1} RANGE

The gas distributions for NH_3, CH_3D, and PH_3 between 0.2 and 1 bar have been inferred from the 180–1300 cm^{-1} portion of the NEB spectrum, using the temperature profile illustrated in Figure 5. The determination of the individual mole fractions from the 850–1300 cm^{-1} interval is difficult due to the overlapping absorption of these gases as illustrated in Figure 6. The homogeneous path spectrum of each gas is computed for the average temperature (125 K), pressure (0.4 bar), and optical pathlength (u in cm atm at NTP) down to 0.8 bar. The absorption by NH_3 is found to dominate from 850 to 1100 cm^{-1}, and by CH_4 from 1180 to 1450 cm^{-1}. The effect of CH_3D is noticeable between 1120 and 1220 cm^{-1} and of PH_3 between 1100 and 1200 cm^{-1}. The strategy adopted to infer the gas distributions from the measured spectrum, while also accounting for these overlapping effects, was to first determine the NH_3 distribution, then the CH_3D distribution using the inferred NH_3, and finally the PH_3 distribution using the inferred NH_3 and CH_3D data. This process was then iterated until all gas distributions converged.

a) *Ammonia* (NH_3)

Gaseous NH_3 is the dominant molecular opacity over a large fraction of the thermal spectrum (see Figs. 3 and 4). Examination of the $1/e$ curve indicates that NH_3 information may be inferred from the IRIS spectrum over 0.2–0.8 bar from 850 to 1100 cm^{-1} and over 0.6–1 bar from 180 to 300 cm^{-1}. Computed spectra assuming the solar value of 1.78×10^{-4} (Lambert 1978) for the well-mixed region and following the NH_3 saturation in the upper troposphere (Fig. 16) are compared to the observed spectra in Figures 7*a* and 8. The comparison for both spectral ranges indicates depletion of NH_3 with respect to the saturation law between 0.2 and 0.8 bar.

At the 0.6–0.8 bar level, common to both spectral ranges, one unique NH_3 distribution should satisfy portions of both spectral ranges which correspond to the common weighting functions. However, an initial attempt to retrieve the NH_3 distribution from both 180–300 and 850–1100 cm^{-1} was unsuccessful as both could not be simultaneously fitted with the same distribution. The fit from 850 to 1100 cm^{-1} was excellent, while the fit from 180 to 300 cm^{-1} was only fair, since the calculated spectra exhibit a slope different from that of the observed. The inferred profiles left residual temperature differences of $\sim$1–2 K for 180–300 cm^{-1}, which is large compared to instrumental noise (0.03 K), whereas from 850–1100 cm^{-1} the residual errors are comparable to the noise level ($\sim$0.7 K). The low wave number spectrum shows a systematic trend with maximum disagreement at the lowest wave numbers. Because of this difficulty at low wave numbers, the NH_3 distribution was inferred from 850 to 1100 cm^{-1} for the 0.2–0.8 bar region; only the continuum in the 180–300 cm^{-1} range was used to derive the well-mixed NH_3 abundance for pressures >0.8 atm.

The NH_3 distribution was inferred using the retrieval algorithm of Smith (1970), iterating until the rms radiance residuals were less than 1%. The retrieved profile (Fig. 16) is close to saturation at the 0.2–0.4 mb

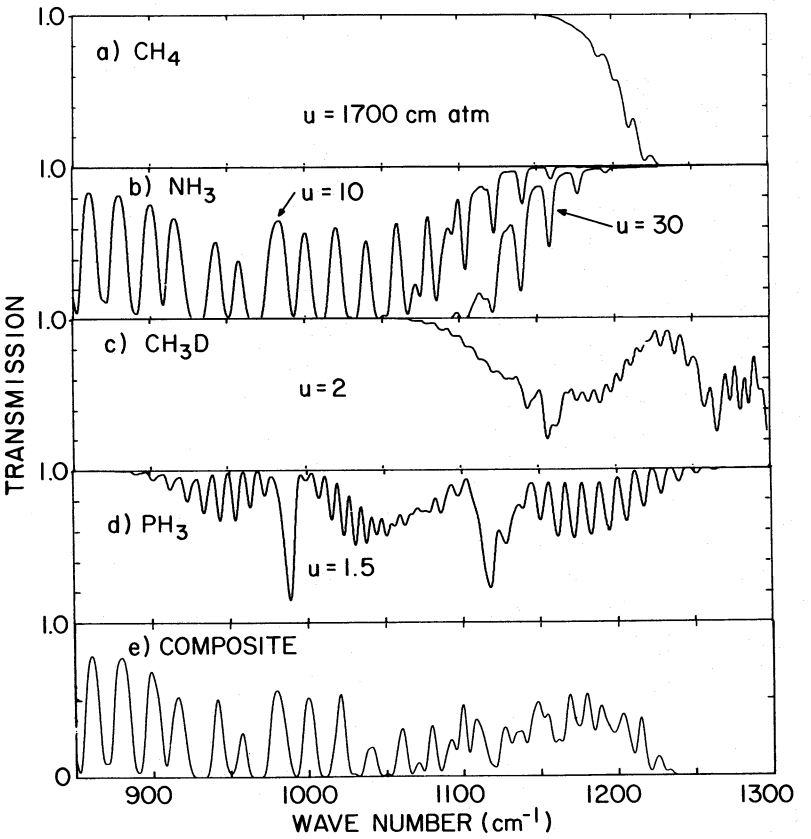

FIG. 6.—Synthetic homogeneous path spectra for the gases in the Jovian atmosphere absorbing in the 850–1300 cm^{-1} region. The transmittances were computed for the average temperature (125 K) and pressure (0.4 bar), and the optical pathlength (u in cm atm at NTP) down to the 0.8 bar level. For NH_3 in Fig. 6*b*, the 850–1125 cm^{-1} region is saturated for $u = 30$ cm atm. To illustrate the NH_3 line structure in this region, the transmittance for $u = 10$ cm atm (corresponding to the 0.5 bar level) is also included, and it is this curve which is included in the composite in Fig. 6*e*. The composite spectrum in Fig. 6*e* illustrates the strong overlapping and blending of these gases at the IRIS 4.3 cm^{-1} resolution.

level, becoming increasingly subsaturated and reaching a depletion factor of ~ 3 at 0.7 bar. This profile then converges with the assumed solar value of $q_{NH_3} = 1.78 \times 10^{-4}$ (Lambert 1978) at ~ 0.8 bar. No stratospheric emission from NH_3 is evident in the centers of the two strong Q branches at 930 and 967 cm^{-1}. The synthetic spectrum corresponding to the inferred profile is also shown in Figures 7*a* and 8.

An estimate of the error in the inferred NH_3 profile has been made for three pressure levels. The random error in the volume mixing ratio, Δq_r, was determined by perturbing the mixing ratio at a given pressure level until the error in the brightness temperature matched the magnitude of the instrument noise, ΔT_I. The error estimates were evaluated (see Table 1) for three wave numbers which were most sensitive to the given pressure levels. The pressure region over which the perturbation was applied is also given in Table 1. For example, at the 0.6 atm level, the maximum perturbation was applied at this level, with the perturbation then decreasing linearly in altitude back to the unperturbed values at 0.4 and 0.8 atm. Thus each perturbation is localized to an altitude range corresponding to approximately 0.2 to 0.3 atm. The larger random error for the 0.3 atm level is caused by the larger ΔT associated with the colder temperatures and smaller temperature gradient at that level. Systematic errors can also be caused by uncertainties in calibration (Δq_1), temperature structure (Δq_2), and molecular parameters (Δq_3). A systematic relative error of 0.1 K in the calibration results in $\Delta q_1/q = 1\%$. An uncertainty in the retrieved profile of $\Delta T = \pm 0.5$ K yields $\Delta q_2/q = 10\%$. The error in the band intensity is estimated to be 5% yielding $\Delta q_3/q = 5\%$. These systematic errors, as well as the total error in the inferred NH_3 distribution, are shown in Table 1. The total error is also illustrated in Figure 16.

The NH_3 mole fraction in the presumably well-mixed portion of the atmosphere ($P > 0.8$ bar) was determined from the three continuum intervals 205–210, 220–230, and 245–250 cm^{-1}. Synthetic comparisons for the 180–300 cm^{-1} range are shown in Figure 7*b* for two values of the well-mixed NH_3 mole fraction, 0.5 solar and 1.5 solar. The synthetic spectra for all three cases show a slope different from that of the observed, with the crossover occurring at ~ 230 cm^{-1}. As the instrument noise level is only ~ 0.03 K at these wave numbers, a

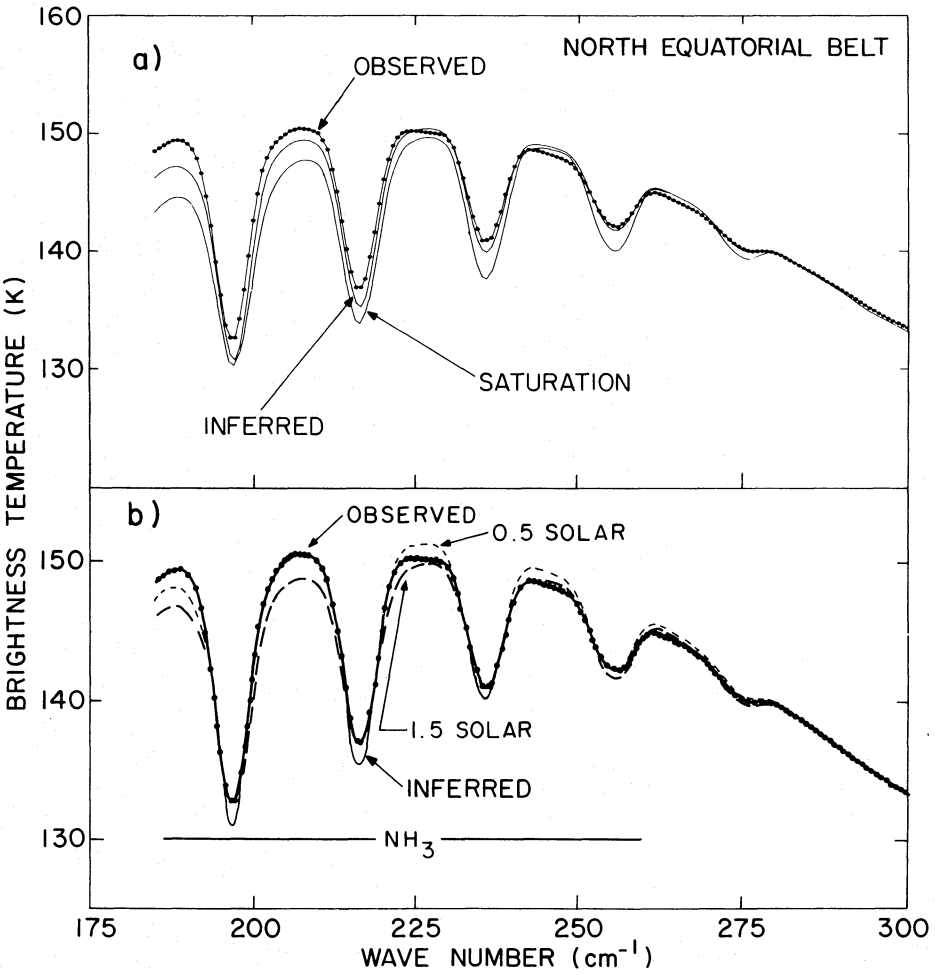

FIG. 7.—Comparison of observed and synthetic spectrum for the 180–300 cm^{-1} region. Fig. 7*a* panel illustrates the effect of the NH_3 distribution on the emergent brightness temperature spectrum in the 0.2–0.8 bar altitude range. Fig. 7*b* panel illustrates the effect of the NH_3 distribution in the well mixed region ($P > 0.8$ bar) on the emergent brightness temperature spectrum, with the solar value of q_{NH_3} being 1.8×10^{-4} (Lambert 1978). The spectrum is sensitive to NH_3 in the well mixed region only in the continua between the absorption lines. The 0.5 solar curve in the 210 cm^{-1} region is obscured by the observed spectrum. The instrument noise level in the observed spectrum is ~0.03 K.

TABLE 1

ERROR ESTIMATES FOR INFERRED NH_3 DISTRIBUTION

PRESSURE LEVEL (RANGE) (bar)	EVALUATION WAVE NUMBER (cm^{-1})	MOLE FRACTION q	RANDOM ERROR[a]		SYSTEMATIC ERROR[a]			TOTAL ERROR[a]
			ΔT_I (K)	$\Delta q_r'$	Δq_1	Δq_2	Δq_3	Δq
0.3 (0.14–0.4)	967	1.4×10^{-6}	0.8	±0.6	±0.01	±0.14	±0.07	±0.6
0.45 (0.25–0.65)	970	8.9×10^{-6}	0.5	±0.5	±0.09	±0.89	±0.45	±1.1
0.6 (0.4–0.8)	980	3.0×10^{-5}	0.2	±0.3	±0.03	±0.30	±0.15	±0.4

[a] The error estimates should be multiplied by the same exponential factor as the mole fraction for that level.

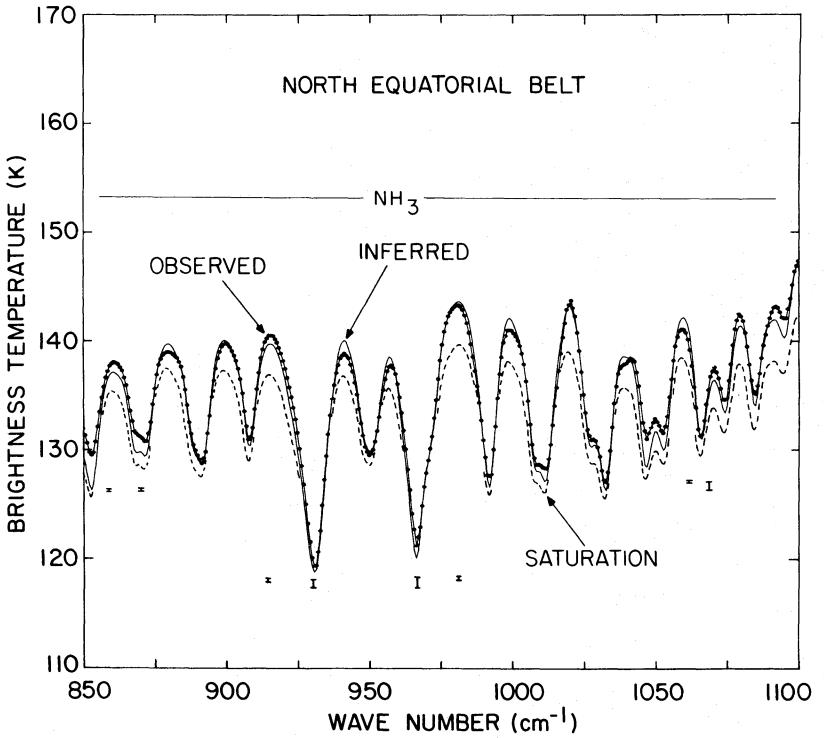

FIG. 8.—Comparison of observed and synthetic spectra for the 850–1100 cm^{-1} region. The best agreement with the observed spectrum is obtained with the inferred NH_3 profile (Fig. 16). Absorption by PH_3 was included using its inferred distribution. The instrument noise level in the observed spectrum is indicated by the small vertical error bars.

large systematic error is indicated. Possible error sources include errors in the instrument calibration, the retrieved thermal structure, and the NH_3-H_2, H_2-H_2, and H_2-He absorption coefficients. The instrument calibration is not as well known below 200 cm^{-1} as above that wave number because of the steep slope at the edge of the instrument response function. Some uncertainty could also come from the retrieved temperature profile since the residuals calculated in the inversion procedure were significantly above the instrument noise level. But probably most important, the NH_3 continuum in the 180–300 cm^{-1} region is mainly formed by the far wings of the strong rotational lines ($\Delta\nu \simeq 50$–100 cm^{-1}) for which the pressure induced H_2-NH_3 line shape is unknown. With this uncertainty it is not possible to infer precisely the NH_3 mole fraction from the low wave number spectrum. Visual comparison of the observed and synthetic spectra in the three continuum regions suggests a value for the well-mixed region which is consistent with the solar value ($q_{NH_3} = 1.78 \pm 0.89 \times 10^{-4}$) and an uncertainty of a factor of 2. Thus the error of the NH_3 mole fraction in the well-mixed region is entirely due to systematic errors in the 180–300 cm^{-1} range.

In principle, information on the NH_3 abundance in the well-mixed region is also available from $\sim$1150 cm^{-1} where the emission originates at about 0.8–0.9 bar. In this spectral range the absorption is mainly

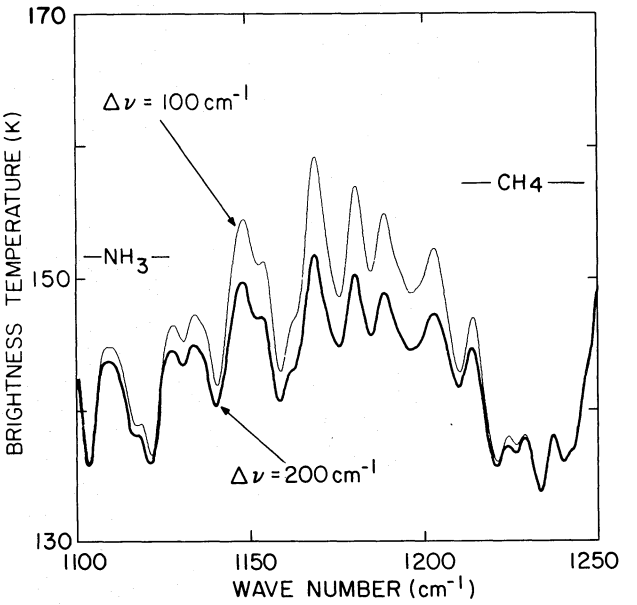

FIG. 9.—Synthetic spectra for the 1100–1250 cm^{-1} region. Absorption by NH_3, CH_4, PH_3, and CH_3D was included using their inferred distribution. The strong effect of the far wing line shape on the location of the continuum is illustrated for two values of the "cut-off" of the Lorentz line shape. The large uncertainty in the far wing line shape, especially for CH_4-H_2 and NH_3-H_2 collisions, is the dominant error source for inferring gas composition from this spectral region.

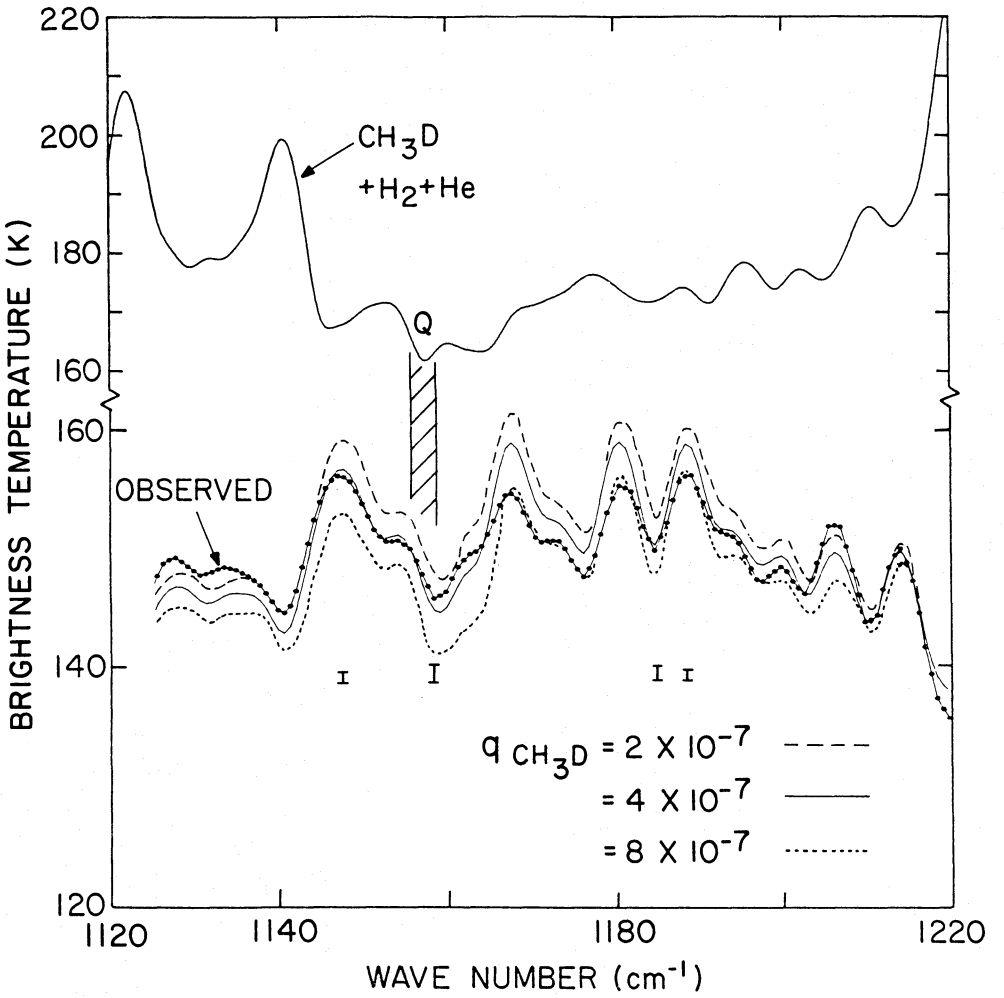

FIG. 10.—Comparison of observed and synthetic spectra to determine q_{CH_3D} from the 1120–1220 cm^{-1} region. Absorption by NH_3, CH_4, and PH_3 was included using their inferred distributions. The uppermost curve has been computed including only the continuum absorption of H_2 and He, and the line absorption of CH_3D to assist in the location of CH_3D features in the observed spectrum. No unique CH_3D lines, including the Q-branch at 1156 cm^{-1}, can be identified in the observed spectrum; thus, the q_{CH_3D} determination depends on matching the observed and synthetic continua. The instrument noise level is indicated by the small vertical bars.

determined by the wings of strong absorption lines of NH_3 and CH_4. As mentioned previously, the value of the absorption in atmospheric windows strongly depends on the assumed line shape for the far wings of collisional broadened lines. An example of the resulting uncertainty is given in Figure 9 where spectra have been computed for all gases for Lorentz cutoffs of 100 and 200 cm^{-1}, which corresponds to ~1000 and 2000 half-widths at the 1 bar level, respectively. The resultant error in the continuum at 1148 cm^{-1} can be as high as 4 K. The large uncertainty in the applicable line shape precludes at the present time derivation of the well-mixed NH_3 mole fraction from this part of the spectrum. Inference of the NH_3 abundance in the well-mixed region is thus limited by uncertainties in the far wing line shape for CH_4-H_2 and NH_3-H_2 collisions.

b) *Deuterated Methane* (CH_3D)

The ν_6 band of CH_3D has absorption features between ~1120 and 1220 cm^{-1} (Fig. 6*c*). Synthetic spectra of Jupiter have been computed for uniformly mixed values of $q_{CH_3D} = 2$, 4, and 8×10^{-7} as shown in Figure 10, all other absorber distributions being unchanged. The calculated spectrum is sensitive to the CH_3D abundance over the 1120–1220 cm^{-1} range, but a detailed comparison with the measured spectrum indicates that all spectral features can be accounted for by CH_4, NH_3, and PH_3. No unique CH_3D line, not even the Q branch at 1156 cm^{-1}, is evident at the 4.3 cm^{-1} resolution. Thus the accurate determination of q_{CH_3D} in this spectral interval depends entirely on the CH_3D band contour. The continuum level in this spectral interval is mainly

established by the far wings of the NH_3 and CH_4 lines, and thus the inferred value for q_{CH_3D} is again sensitive to assumptions concerning the far-wing line shape, as illustrated by Figure 9. To test this sensitivity further, we have calculated synthetic spectra for various values of the Lorentz cutoff up to 2000 half-widths for all absorbers, keeping all abundances unchanged. It was observed that the calculated spectrum was constant when the Lorentz cutoff reached values higher than about 1800 half-widths. Varying then the CH_3D abundance, the best fit with the observed spectrum leads to a mixing ratio $q_{CH_3D} = 2.7 \times 10^{-7}$, which is thus a lower limit. Taking into consideration the instrument noise (0.7 K), the error is $\pm 0.5 \times 10^{-7}$. Note that this lower limit is conservative since it implies a very unlikely high value of the far-wing CH_4 contribution (Gautier *et al.* 1982). More definitive determination of CH_3D from the 1156 cm^{-1} band will require data with higher spectral resolution than 4.3 cm^{-1} and more accurate knowledge of the NH_3-H_2 and CH_4-H_2 continuum absorption. Better laboratory measurements of line shape parameters are badly needed.

c) *Phosphine* (PH_3)

Information on the PH_3 concentration in the upper troposphere may be derived from the 1100–1200 cm^{-1} interval where the ν_4 band of PH_3 has a strong influence (Fig. 6*d*). Synthetic spectra for two PH_3 distributions (see Fig. 17) are compared to the IRIS observations in Figure 11. Distribution 1 represents the effect of PH_3 photochemistry only, while the inferred distribution is similar to distribution 2 which includes PH_3-NH_3 coupling (Strobel 1977). Both distributions are normalized in the deep atmosphere to the average value inferred from the 2100–2250 cm^{-1} region (6×10^{-7}). The 1100–1200 cm^{-1} range is sensitive to the PH_3 distribution between about 0.4 and 0.8 bar. The uppermost curve of Figure 11 has been computed with only H_2, He, and the inferred PH_3 distribution to aid in the identification of the PH_3 lines used in the analysis. The *Q*-branch at 1119 cm^{-1} is heavily blended by the NH_3 multiplet; however, it is still valuable as a diagnostic line for determining the PH_3 abundance. Fairly isolated PH_3 *P*-branch multiplets are seen to occur at 1131, 1152, and 1163 cm^{-1} (lines 2, 3, and 4).

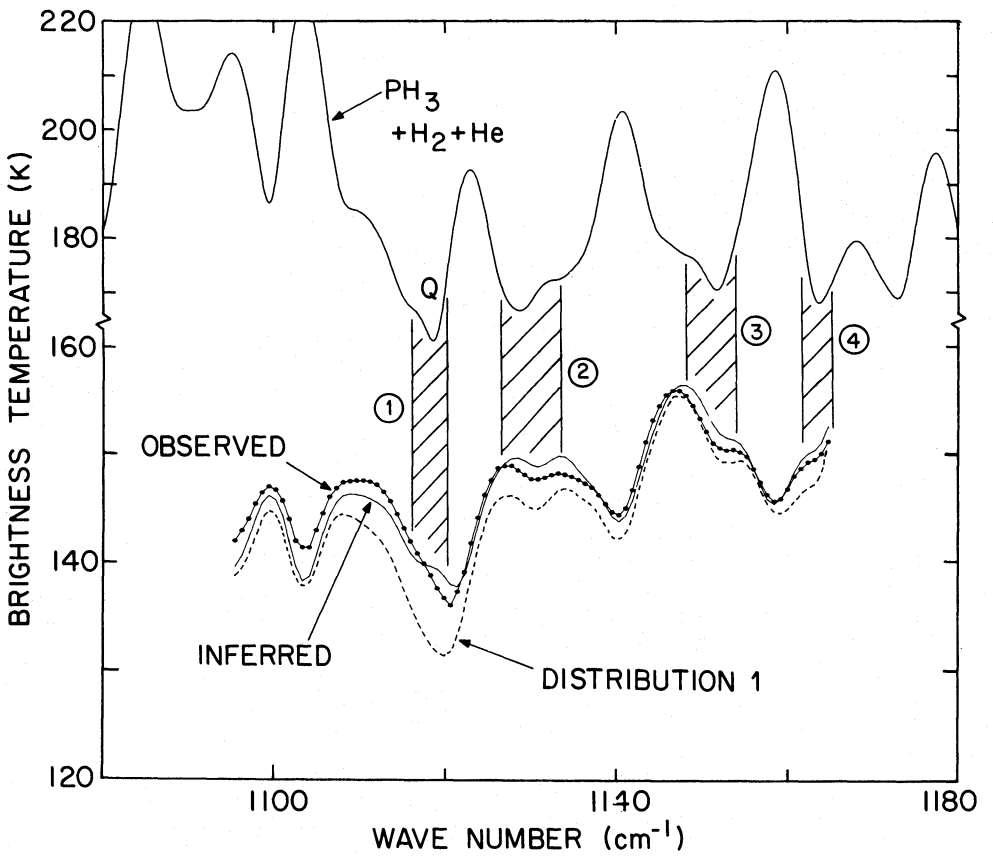

FIG. 11.—Comparison of observed and synthetic spectra to determine q_{PH_3} from 1080–1180 cm^{-1} region. The PH_3 distributions are shown in Fig. 17. Absorption by NH_3, CH_4, and CH_3D was included using their inferred distributions. The uppermost curve has been computed, including only the continuum absorption of H_2 and He, and the line absorption of PH_3 to assist in the location of PH_3 features in the observed spectrum. Four of the PH_3 multiplets used in the analysis are indicated by the vertical crosshatched regions. The instrument noise level is indicated by the small vertical bars.

Comparison of the synthetic and observed spectra show that distribution 1 overestimates the PH_3 absorption at all wave numbers, especially near the Q-branch at 1119 cm^{-1}. The inferred distribution, with considerably less PH_3 in the upper troposphere, gives fair agreement for most of the PH_3 features. The remaining discrepancy in the continuum is thought to be due to the errors in the assumed far wing contribution of CH_4 and NH_3 and the CH_3D abundance as discussed before. The error bars shown in Figure 17 reflect the uncertainty due to instrument noise.

V. GAS DISTRIBUTIONS FROM THE 1800–2250 cm^{-1} RANGE

The vertical distributions for PH_3, CH_3D, H_2O, and GeH_4 between 1 and 5 bars have been inferred from the 1800–2250 cm^{-1} portion of the NEB spectrum (Fig. 2). As between 850 and 1300 cm^{-1}, the determination of individual mixing ratios is difficult due to overlapping absorption of these gases. This blending is illustrated by the homogeneous path spectra of Figure 12; the spectrum for each gas is computed for the average temperature (200 K), average pressure (1.25 bar), and optical pathlength (u in cm atm at NTP) down to the 2.5 bar level. Absorption by NH_3 dominates from 1800 to 1900 cm^{-1}, by H_2O from 1900 to 2100 cm^{-1}, and by PH_3 from 2100 to 2250 cm^{-1}. CH_3D influences the 2100–2200 cm^{-1} interval. The previously inferred NH_3 distribution (Fig. 16) was adopted for the analysis in the 1800–2250 cm^{-1} range. The NH_3 concentration in the deep atmosphere cannot be inferred from the 1800–1900 cm^{-1} spectrum because of large uncertainties in the NH_3 band strength and far-wing contribution of the ν_4 band at 1627 cm^{-1}; furthermore, the strength for the $2\nu_2^s$ NH_3 band at 1882 cm^{-1} is not available at all. A lower limit of $S_b = 0.02$ cm^{-2} atm^{-1} has been determined for the $2\nu_2^s$ band from the IRIS spectrum, using the previously inferred NH_3 distribution. Future improvements of the NH_3 absorption parameters for ν_4 and $2\nu_2^s$ will allow the NH_3 distribution in the lower

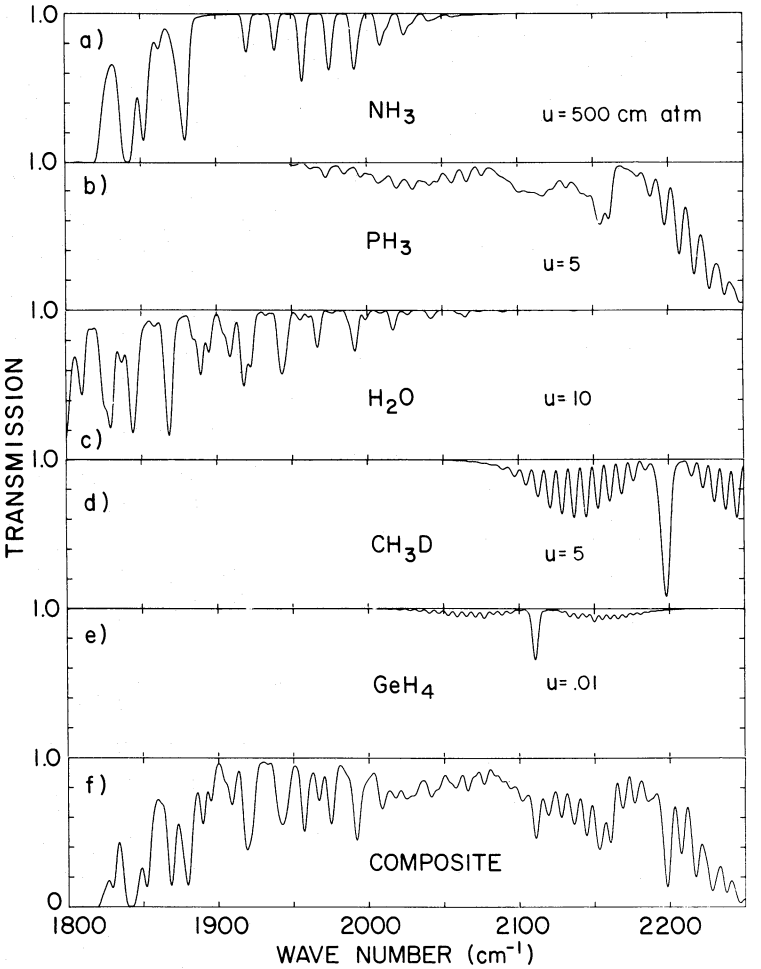

FIG. 12.—Synthetic homogeneous path spectra for the gases in the Jovian atmosphere in the 1800–2250 cm^{-1} region. The transmittances were computed for the average temperature (200 K) and pressure (1.25 bar), and the optical path length (u in cm atm at NTP) down to the 2.5 bar level in the Jovian atmosphere. The composite spectrum in Fig. 12f illustrates the strong overlapping and blending of the gases at the IRIS 4.3 cm^{-1} resolution.

atmosphere to be determined from the 1800–1900 cm^{-1} spectrum. The strategy adopted in this analysis was first to determine the distribution of PH_3, then CH_3D, then GeH_4, and finally H_2O.

The computed spectra shown in Figures 13, 14, and 15 include the effect of a gray absorbing haze. Spectra computed including only molecular absorption show maximum brightness temperatures of ~270 K, about 10 K higher than the observed temperatures. At the present time, insufficient knowledge of the cloud and haze structure and their optical properties prevents construction of more accurate models of the opacity; therefore, we have modeled the cloud and haze continuum in the simplest way, which is a uniformly mixed gray haze. The haze scale height was taken equal to the gas scale height ($H_h = 35$ km), with the quantity $\sigma N(z_0)$ determined by normalizing the computed and observed spectra at 2085 cm^{-1}, the region of greatest molecular transparency. The base of the haze layer was taken at 5 bars ($z_0 = 0$ km). The optical depth of the haze equals 0.54 at 5 bars (279 K). The effect of the haze on the atmospheric transmittances and brightness temperatures may be seen in Figures 4 and 15*b*, respectively. This ad hoc haze model fits the observed spectrum satisfactorily to first order and, therefore, gives some confidence that it is adequate for inferring molecular gas abundances. The haze model is obviously not unique, and other types of haze or cloud models could be developed to account for the residual continuum. The uncertainties in the derived gas distributions from the haze model uncertainties are not quantitatively assessed in this paper, but a rough estimate of the error is included in the total error estimates.

a) Phosphine (PH_3)

Absorption by PH_3 affects the spectrum from 2050–2225 cm^{-1}, as illustrated in Figure 13. The spectrum in Figure 13*a* has been computed including only continuum absorption (H_2, He, CH_4, haze) and the PH_3 absorption, to aid in the identification of PH_3 lines in the observed spectrum. Figure 13*b* shows the comparisons of the observed spectrum to synthetic spectra with PH_3 mole fractions of 4×10^{-7} and 8×10^{-7}. The synthetic spectra in Figure 13*b* include the effects of all other absorbing gases, besides PH_3, at their inferred concentrations and the gray haze. The absorption features in the observed spectrum which are strongly influenced by individual PH_3 multiplets are

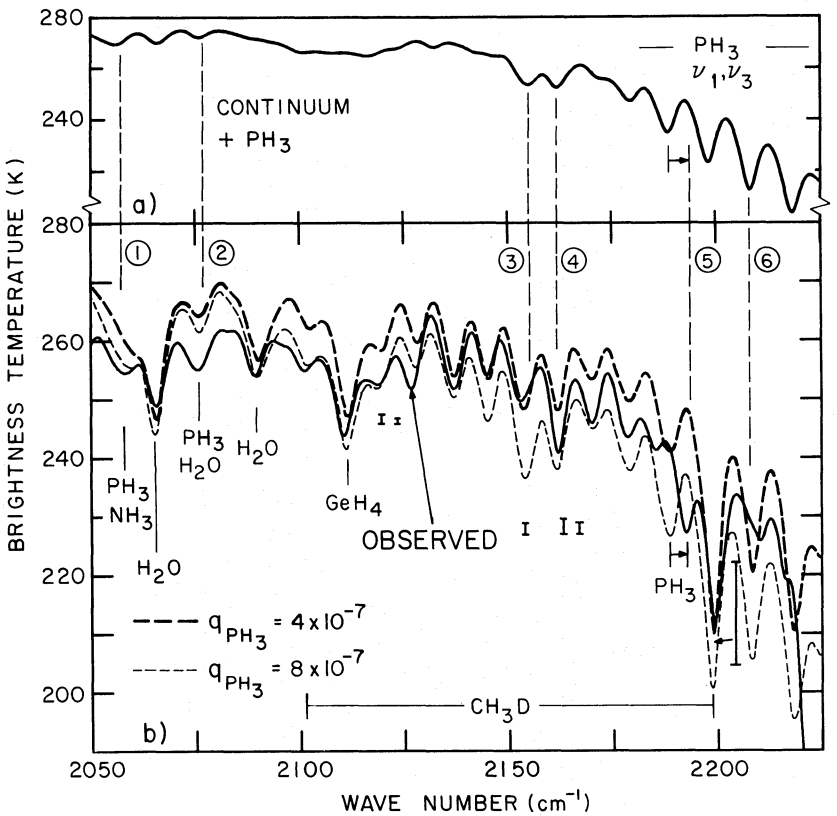

FIG. 13.—Comparison of observed and synthetic spectra to determine q_{PH_3} from the 2050–2225 cm^{-1} region. Absorption by NH_3, H_2O, GeH_4, and CH_3D was included using their inferred distributions. The uppermost curve has been computed including only the continuum absorption of H_2, He, CH_4, and the aerosol, and the line absorption of PH_3 to assist in the location of PH_3 features in the observed spectrum. The mole fraction of PH_3 is determined from the line to continuum ratio for multiplets (3) and (4), and the continuum roll-off from 2170 to 2225 cm^{-1}. The instrument noise level is indicated by the small vertical bars underlying the spectra.

indicated by the vertical dashed lines, numbered 1 through 6. Only line 5 is isolated and unblended; this line is displaced in the synthetic spectrum and should be shifted to higher wave numbers by the increment shown by the short horizontal arrow in Figures 13*a* and 13*b*. This error results from inadequate theoretical line positions for the high J lines of the ν_1 and ν_3 fundamentals. The shifted position agrees with laboratory data. Multiplet 1 is blended with a weak NH_3 line; multiplet 2, with a weak H_2O line; and multiplets 3, 4, and 6 are blended with CH_3D lines. The PH_3 mole fraction was determined from spectral comparisons in two regions: (1) 2150–2170 cm^{-1}: The line-to-continuum ratio for multiplets 3 and 4 indicates a PH_3 mole fraction from 4 to 8 $\times 10^{-7}$, and (2) 2170–2225 cm^{-1}: The roll-off of the continuum from 2170 cm^{-1} to 2225 cm^{-1}, along the P-branch contour of the ν_1 and ν_3 fundamental bands, also indicates $q_{PH_3} = 4$–8×10^{-7}. As the same q_{PH_3} value satisfies both diagnostic spectral regions, we adopt $q_{PH_3} = 6 \pm 2 \times 10^{-7}$ as the mean value for the 1–4 bar region.

b) *Deuterated Methane* (CH_3D)

Absorption lines of the ν_2 band of CH_3D dominate most of the observed spectrum from 2100 to 2200 cm^{-1}. The synthetic spectra of Figure 14*b* have been computed for CH_3D mole fractions of 1×10^{-7} and 5×10^{-7}, including the gray haze and the other absorbing gases with their inferred concentrations. The CH_3D mole fraction has been determined from comparison of the observed and synthetic spectra in two regions: (1) 2120–2145 cm^{-1}: Four unblended multiplets of the ν_2 P-branch ($P10$–$P7$) lie in this region. Comparison of the line to continuum ratio gives best agreement with $q_{CH_3D} = 4$–5×10^{-7} (multiplet 1 [$P10$] does not even appear above the continuum for $q_{CH_3D} = 1 \times 10^{-7}$); (2) 2200 cm^{-1}: The Q-branch of the ν_2 band at 2200 cm^{-1} fits best for $q_{CH_3D} = 1 \times 10^{-7}$. The instrumental noise ($\Delta T = \pm 9$ K) allow q_{CH_3D} to range from 0.5 to 4×10^{-7} for the Q-branch region.

The P-branch lines require a higher value of q_{CH_3D} (4–5×10^{-7}) and the Q-branch, a lower value (0.5–4×10^{-7}). This difference probably reflects mostly the uncertainties with establishing the continuum. We adopt $q_{CH_3D} = 3.5^{+1.0}_{-2.5} \times 10^{-7}$, to include the range of possible values for both P- and Q-branch lines.

c) *Germane* (GeH_4)

The strong Q-branch of the ν_3 band of GeH_4 absorbs significantly near 2111 cm^{-1} (Fig. 15). This feature is

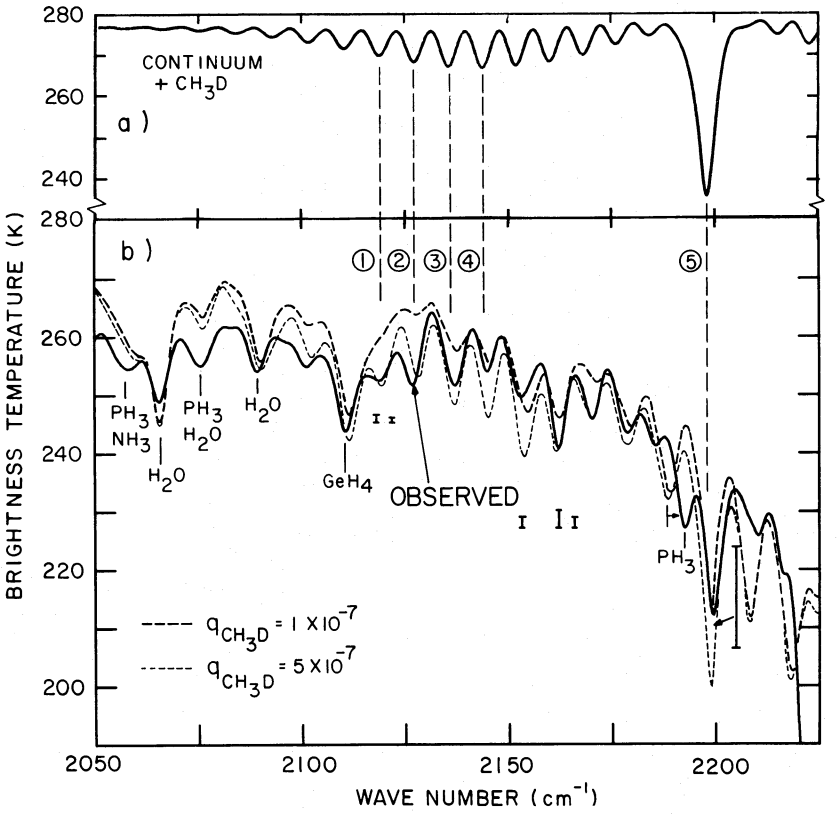

FIG. 14.—Comparison of observed and synthetic spectra to determine q_{CH_3D} from the 2050–2225 cm^{-1} region. Absorption by NH_3, H_2O, GeH_4, and PH_3 was included using their inferred distributions. The uppermost curve has been computed including only the continuum absorption of H_2, He, CH_4, aerosol, and the line absorption of CH_3D to assist in the location of CH_3D features in the observed spectrum. The mole fraction of CH_3D is determined from the line to continuum ratio for P branch multiplets (1) through (4) and the Q branch (5). The instrument noise level is indicated by the small vertical bars underlying the spectra.

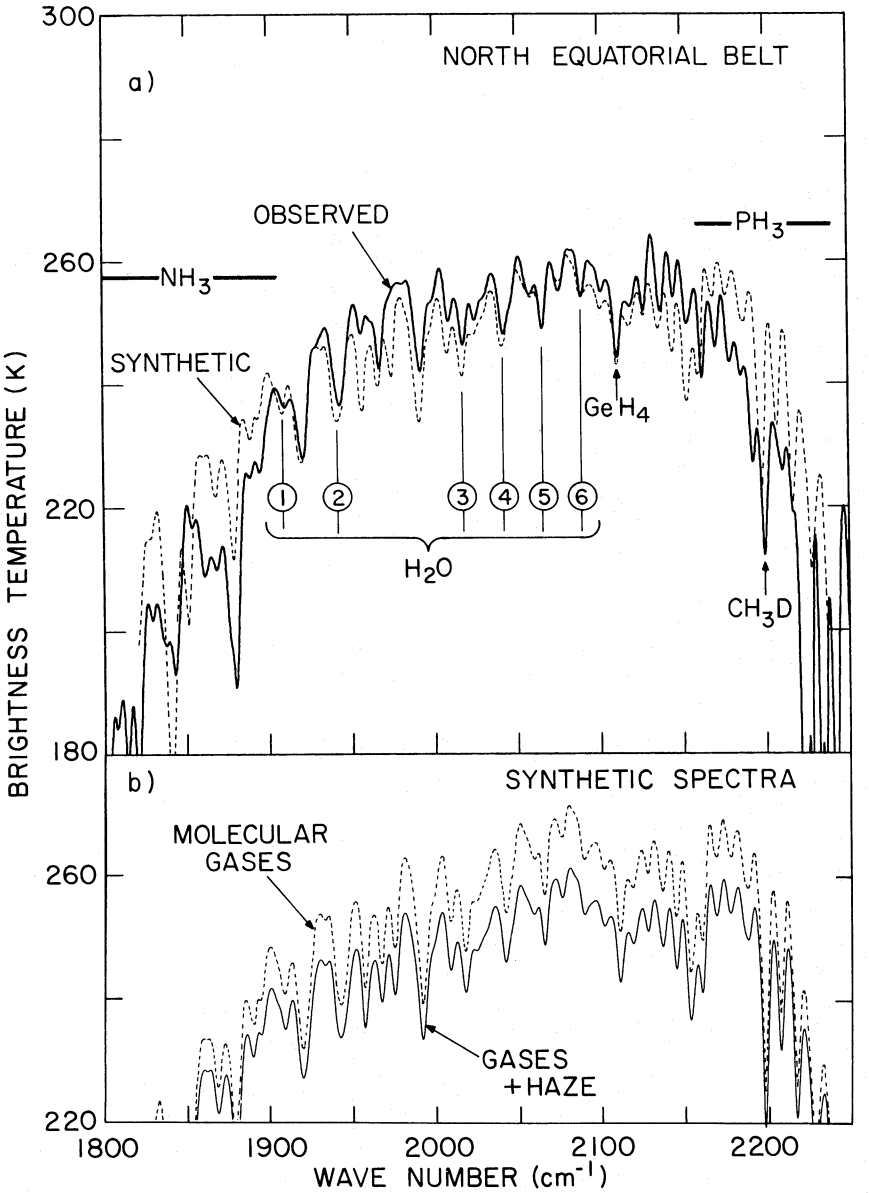

FIG. 15.—(*a*) Comparison of observed and synthetic spectra for the 1800–2250 cm^{-1} region. The mole fraction of H_2O has been determined from the 1875–2100 cm^{-1} region using the six H_2O multiplets indicated. Absorption by NH_3, PH_3, GeH_4, and CH_3D was included using their inferred distributions. (*b*) The effect of the well mixed gray haze is illustrated. The optical depth of the haze is 0.54 at 5 bar (279 K).

fairly well isolated from surrounding weak H_2O, CH_3D, and individual PH_3 lines, but it is overlapped by the continuum formed by many weak PH_3 lines (Fig. 12). The weak *P* and *R* lines of GeH_4 are all masked by stronger PH_3 and CH_3D lines and are not apparent in the spectrum. The appearance of the *Q*-branch but not of any *P* or *R* lines in the IRIS spectrum agrees with the higher spectral resolution measurements by Fink, Larson, and Treffers (1978). Comparisons of synthetic with the observed IRIS spectra for the *Q*-branch yield $q_{GeH_4} = 7 \pm 2 \times 10^{-10}$.

d) Water Vapor (H_2O)

The high *J* lines of the ν_2 band of H_2O influence the 1900–2100 cm^{-1} interval (Figs. 12 and 15). All 14 H_2O features identified by Larson *et al.* (1975) in the initial detection of H_2O in the Jovian atmosphere are evident in the IRIS spectrum. Six of the fairly isolated H_2O lines are indicated in Figure 15*a*. Comparisons to synthetic spectra indicate $q_{H_2O} = \sim 1 \times 10^{-6}$ at 2.5 bars increasing to $\sim 3 \times 10^{-5}$ at 4 bars. These values should be good to approximately a factor of 2. The synthetic

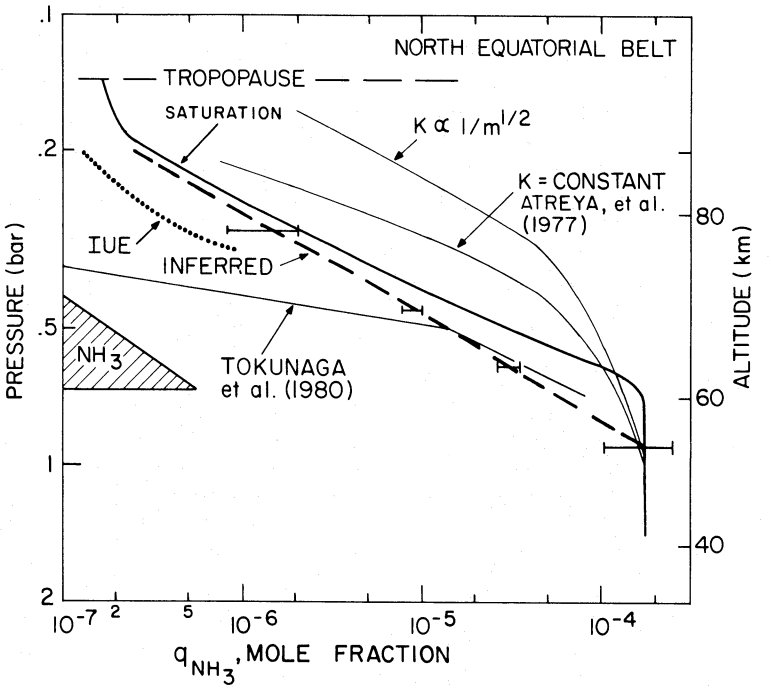

FIG. 16.—Altitude profiles for gaseous NH_3 in the NEB. The inferred distribution, which gives the best fit to the IRIS spectrum, is subsaturated in the upper troposphere. In the region below 1 bar, agreement is found with the solar value of Lambert 1978. The NEB distribution from Tokunaga, Knacke, and Ridgway (1980) was derived from ground-based infrared measurement. The spatially resolved *IUE* distribution corresponds to the Equatorial Zone, not the NEB. The model atmosphere predictions of Atreya *et al.* 1977 are included to illustrate the capability of one-dimensional photochemical models to explain the observed distributions. A quantitative comparison between the observed and model distributions should not be made, as the globally averaged model distributions are not appropriate for the spatially resolved NEB.

spectrum corresponding to this distribution is shown in Figure 15*a*.

VI. GAS COMPOSITION—DISCUSSION

a) *Ammonia* (NH_3)

Ammonia plays an important role in the understanding of the Jovian atmosphere: it is the only observed constituent containing N, thus permitting analysis of the elemental abundances of nitrogen; it must play a role in chemical processes with the detailed reactions still unknown; it is the dominant constituent of the upper clouds; and it is important to meteorology and dynamics because of release and consumption of latent heat in phase changes.

The NH_3 distribution inferred in this investigation is shown in Figure 16. The vertical distribution of NH_3 in the Jovian atmosphere has been the subject of numerous investigations using ground-based data (Baluteau *et al.* 1980; Encrenaz, Combes, and Zeau 1980; Marten *et al.* 1980; Gautier *et al.* 1979; Goorvitch *et al.* 1979; Tokunga *et al.* 1979; Baluteau *et al.* 1978; Erickson *et al.* 1978; Ridgway, Wallace, and Smith 1976; Lacy *et al.* 1975); however, these measurements have all been at low spatial resolution, usually for averages over the entire disk, and are therefore not directly comparable to the IRIS NH_3 distribution which is derived for the NEB. Only the recent observations of Tokunaga, Knacke, and Ridgway (1980) resolved the NEB; therefore, their derived NH_3 profile is shown in Figure 16. Fair agreement exists for the 0.5–0.7 bar range with serious differences apparent for lower pressures. The reasons for this discrepancy are not known. The difference does not appear to be in either set of observations as the *Q*-branch (930 and 970 cm^{-1}) temperatures in both measurements are approximately the same (120 K). Differences must therefore be a consequence of different assumptions in the models. Knacke *et al.* (1982) have derived $q_{NH_3} = 3.0 \pm 1.5 \times 10^{-4}$ for the well-mixed region of the center of the disk (4.″3 beam) from $\Delta\nu = 1$ cm^{-1} spectra in the 1100–1200 cm^{-1} range. A spatially resolved (3″) vertical distribution of NH_3 in the upper atmosphere has been obtained from *IUE* observations (Combes *et al.* 1981) for the Equatorial Zone of Jupiter. The lower portion of this distribution is also shown in Figure 16. Taking into consideration both errors in the *IUE* measurement and the possible zone-belt difference in upper atmosphere NH_3, the agreement with the IRIS results is acceptable.

The tropospheric distribution of gaseous NH_3 is controlled by several physical mechanisms; dynamics, phase change and photochemistry. Present atmospheric models do not incorporate all three physical mechanisms simultaneously and thus are unable to predict realistic NH_3 distributions for comparison to data. Additionally,

models have only been derived for disk averaged conditions. Two globally averaged representative models from Atreya, Donahue, and Kuhn (1977) are included in Figure 16 for different assumptions for the eddy diffusion coefficient (K), K = constant, and $K \propto 1/m^{1/2}$, where m is the total atmospheric number density. The assumed mixing ratios have been normalized in the deep atmosphere to Lambert's solar value. This comparison should only be made qualitatively as the model conditions, such as solar flux at encounter and spatial resolution, are not appropriate for the *Voyager* conditions. However, it is apparent that comparison of measurements with more comprehensive atmospheric models may yield physical parameters, such as the eddy diffusion coefficient.

It must be emphasized that this depleted NH_3 distribution refers only to the belt region on Jupiter where downward motion is expected to take place. The NH_3 distribution appears to be variable over the planet, with saturation occurring in the upwelling cloudy zones (Marten *et al.* 1981).

b) *Phosphine* (PH_3)

Phosphine is an important trace gas because of its role in both dynamics and chemistry, and its possible association with coloration. Furthermore, PH_3 is an important indicator of nonequilibrium chemical activity in the lower atmosphere, being one of the gases that should not exist in the observable atmosphere on the basis of thermochemical equilibrium models.

The PH_3 distribution inferred in this investigation is shown in Figure 17. PH_3 was first detected in the 1000 cm^{-1} range by Ridgway, Wallace, and Smith (1976) and in the 2100 cm^{-1} range by Larson, Treffers, and Fink (1977) with mole fractions consistent with the solar value of P/H. Beer and Taylor (1979) found PH_3 to be 5–8 times lower than Larson, Treffers, and Fink (1977). The first evidence of PH_3 depletion in the upper troposphere came from Encrenaz, Combes, and Zeau (1978), Tokunga *et al.* (1979), and Encrenaz, Combes, and Zeau (1980), who found mole fractions of $\sim 1\text{–}2 \times 10^{-7}$ in the 0.2–0.6 bar range. Our results are in agreement with the PH_3 depletion in the upper troposphere and with the Larson, Treffers, and Fink (1977) value in the deep atmosphere. Knacke *et al.* (1982) have derived $q_{PH_3} = 7.5 \pm 1.8 \times 10^{-6}$ for the deep atmosphere.

The PH_3 photochemistry was first discussed by Prinn and Lewis (1975), who assumed strong vertical mixing to explain the presence of PH_3 at the 0.4–4 bar level. Strobel (1977) has pointed out that the NH_3 and PH_3 photochemistry are coupled since both constituents are photolyzed by the same UV radiation at a given pressure level. His calculations indicate that the presence of NH_3 increases the photochemical removal of PH_3 through reactions of NH_3 photolysis products H and NH_2 with PH_3. The photochemical model predictions of Strobel (1977) are included in Figure 17, where distribution 1 is for phosphine photochemistry only, and distribution 2 is for the coupled photochemistry of PH_3 and NH_3. The inferred PH_3 distribution compares favorably with distribution 2. The accuracy of the photochemical model is limited by insufficient knowledge of the key reactions and the reaction rates. Furthermore, the models apply to

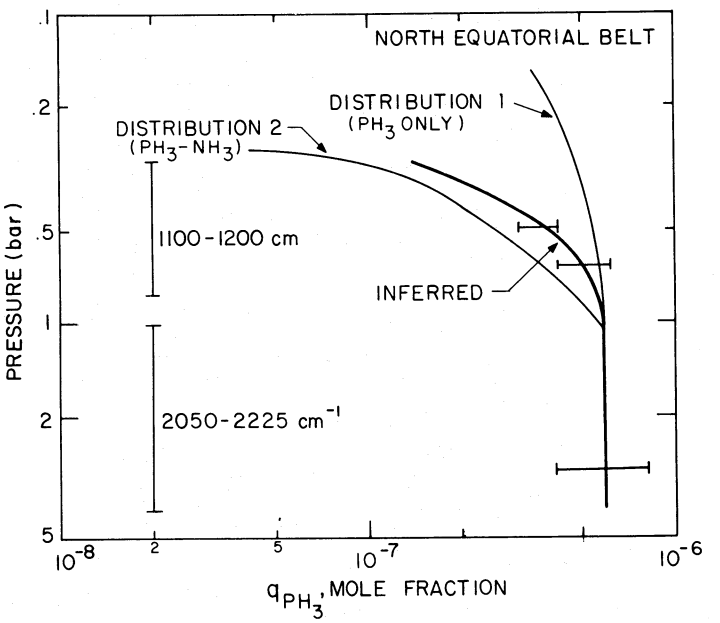

FIG. 17.—Altitude profiles for gaseous PH_3 in the NEB. The inferred distribution represents the best fit to the IRIS spectrum. Distributions 1 and 2 are photochemical model predictions of Strobel 1977 normalized in the deep atmosphere to the value of $q_{PH_3} = 6 \times 10^{-7}$ determined in this investigation. Distribution 1 represents the PH_3 photochemical model of Prinn and Lewis (1975). Distribution 2 includes the coupled photochemistry of NH_3 and PH_3.

mean global conditions rather than to a belt, and the eddy diffusion coefficient is not known. It is assumed to be constant, $K = 2 \times 10^4$ cm^2 s^{-1}, for distributions 1 and 2 (Fig. 17). More definitive conclusions from comparison of theoretical and observed PH_3 distributions require improved models.

c) *Deuterated Methane* (CH_3D)

Deuterated methane is important as a tracer for the evolution of Jupiter, the solar system, and the Galaxy as well as for cosmology. Figure 18 shows the CH_3D mole fraction inferred by this investigation. The lower limit of $q_{CH_3D} = 2.7 \pm 0.5 \times 10^{-7}$ was derived from 1120 to 1220 cm^{-1}, and the value $q_{CH_3D} = 1\text{–}4.5 \times 10^{-7}$ from 2100 to 2200 cm^{-1}. We have adopted a central value of 3.5×10^{-7} along with the upper limit of 4.5×10^{-7} from 2100 to 2200 cm^{-1}, and the lower limit of 2.2×10^{-7} from 1120 to 1220 cm^{-1}. The final adopted value for this investigation is $q_{CH_3D} = 3.5^{+1.0}_{-1.3} \times 10^{-7}$. Drossart *et al.* (1982) have derived a comparable value ($1.8^{+1.4}_{-0.9} \times 10^{-7}$) from an IRIS average spectrum from 2100 to 2200 cm^{-1}, the average consisting of several thousand individual spectra distributed over the Jovian disk.

The first detection of deuterium in the Jovian atmosphere was the measurement of the ν_2 band of CH_3D in the 2100–2200 cm^{-1} interval (Beer and Taylor 1973). They inferred a value of $q_{CH_3D} = 4.8^{+2.7}_{-1.9} \times 10^{-7}$ from a total CH_3D column abundance of 1.3 ± 0.3 cm atm. For internal consistency we have revised this mole fraction by scaling their total CH_3D column abundance to our model atmosphere. The air mass correction of 2 originally included by Beer and Taylor (1973) was not used in our redetermination, in accordance with the revised limb correction given by Beer and Taylor (1978). The revised total CH_3D column abundance is 2.6 ± 0.3 cm atm, and the revised value for q is $q_{CH_3D} = 1.9^{+1.1}_{-0.7} \times 10^{-7}$. A second set of improved measurements of the ν_2 CH_3D band by Beer and Taylor (1978) yields $q_{CH_3D} = 2.9^{+1.7}_{-1.2} \times 10^{-7}$ derived from a column abundance of 4.0 ± 1.0 cm atm, after normalization to our model atmosphere. Our determination of CH_3D is consistent with the Beer and Taylor values at 3 bars. Encrenaz, Combes, and Zeau (1980) have used ground-based observations of the ν_6 band at 1156 cm^{-1} to set an upper limit for q_{CH_3D} less than 1.8×10^{-7} at 0.4 bar. This value is somewhat lower than the IRIS lower limit of $2.7 \pm 0.5 \times 10^{-7}$. One plausible explanation is that the discrepancy arises from the low spatial resolution of the Encrenaz, Combes, and Zeau (1980) observations and the subsequent spectrum modeling which includes the continuum opacity of an ice cloud model. It is quite possible that the cloud opacity has lowered the line-to-continuum ratio, thus leading to a lower CH_3D abundance. Knacke *et al.* (1982) have inferred $q_{CH_3D} = 3.6 \pm 0.54 \times 10^{-7}$ from $\Delta\nu = 1$ cm^{-1} measurements in the 1100–1200 cm^{-1} region.

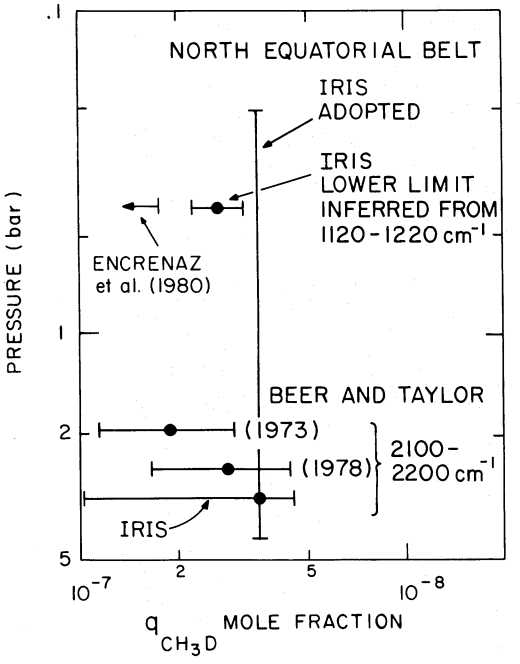

FIG. 18.—The mole fraction of CH_3D as determined from the ν_6 band (1100–1200 cm^{-1}) at 0.6 bar and from the ν_2 band (2100–2225 cm^{-1}) at ~3 bar. The adopted curve represents the best value of q_{CH_3D} as determined from this investigation.

d) *Germane* (GeH_4)

The calculations of Barshay and Lewis (1978) indicate GeH_4 should not be detectable at the 2–5 bar level under chemical equilibrium conditions. Therefore, germane is important as a tracer of vertical motions and nonequilibrium chemistry in the deep atmosphere.

The value of q_{GeH_4} inferred in this investigation is $7 \pm 2 \times 10^{-10}$, which is similar to the value derived from ground-based observations of 6×10^{-10} (Fink, Larson, and Treffers 1978). This value is a factor of ~10 lower than the solar value (Cameron 1973). The observed abundance of GeH_4 is consistent with chemical models only if vertical mixing rapidly convects GeH_4 from the ~1000 K up to the ~250–300 K level. The physical significance of detectable amounts of GeH_4 at 2–5 bars have been discussed by Fink, Larson, and Treffers (1978) and Barshay and Lewis (1978).

e) *Water Vapor* (H_2O)

Water vapor is a trace gas in the lower Jovian atmosphere and is important for elemental abundances, as it is the dominant oxygen-bearing molecule so far identified, and for meteorology and dynamics, as it liberates and consumes latent heat while changing phase.

This investigation inferred a H_2O concentration of $\sim 1 \times 10^{-6}$ at the 2.5 bar level and gradually increasing to $\sim 3 \times 10^{-5}$ at 4 bars. The initial detection of H_2O from aircraft disk observations was by Larson *et al.* (1975) who derived a value of $\sim 1 \times 10^{-6}$ from comparison with laboratory spectra. Somewhat higher values have been derived from these observations by Bjoraker *et al.* (1981) using radiative transfer techniques. The general decrease in the H_2O mole fraction with

increasing altitude is consistent with a belt being a down-welling region depleted in its condensible gases. Our mole fraction at the 4 bar level is approximately a factor of 30 lower than the solar value (Cameron 1973). It is conceivable that the water vapor abundance may reach solar proportions at deeper levels (5–10 bars) below the down-welling convective cell or in the zones which cannot be probed because of opaque clouds. If our mole fraction is representative of the bulk atmosphere, and if the atmosphere is representative of the bulk composition of the planet, Jupiter shows a significant depletion in oxygen. An alternate explanation postulates excess of water in zones; the total H_2O content of the atmosphere as a whole may, therefore, still be solar-like (Larson *et al.* 1975).

VII. D/H ISOTOPIC RATIO

The D/H ratio is important as it yields information on chemical processes in the Jovian atmosphere. Additionally, if the deuterium in the primordial solar nebula in the vicinity of the outer planets did not undergo transformation to He^3, then the Jovian value should be representative of the solar system at its formation. Due to difficulties in deriving an accurate D/H ratio for the protosolar nebula from solar composition and wind measurements, the Jovian D/H ratio probably yields the best estimate of D/H in the protosolar nebula. According to astrophysical theory (Epstein, Lattimer, and Schramm 1976) deuterium originated in the big bang, with only modest destruction during subsequent galactic evolution. Observations of the D/H ratio in the planets, meteorites, and interstellar medium, as well as the cosmological significance have been discussed by Schramm and Wagoner (1974) and Geiss and Reeves (1981). The current state of deuterium abundances is summarized in Table 2 and Figure 19 for the solar system and the interstellar medium. The shaded area is defined by the 1 σ error bars from this investigation. The mass fraction (X) is related to the number fraction by $X = 1.63$ D/H for a He/H ratio of 0.055.

The D/H ratio has been found to vary significantly between the highly fractionated objects of the inner solar system (Earth, carbonaceous chondrites) and the unfractionated objects of the outer solar system (Jupiter, Saturn, Uranus). Comparisons have indicated an enhancement in D/H of 4–10 for the Earth (Craig 1961; see summary in Geiss and Reeves 1981) and 7–40 for carbonaceous chondrites (Boato 1954; Robert, Merlivat, and Javoy 1977, 1978, 1979; Kolodny, Kerridge, and

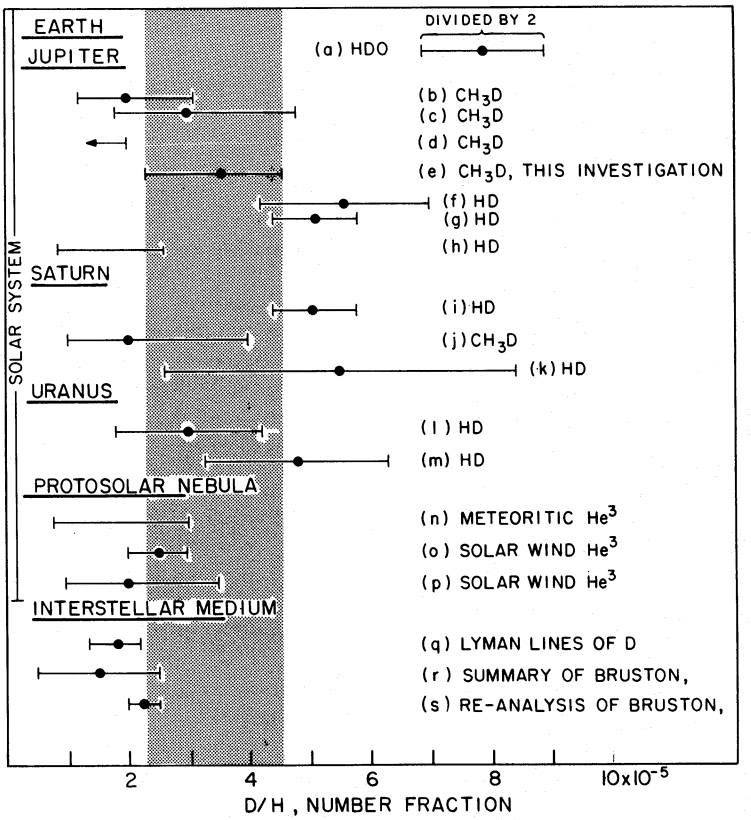

FIG. 19.—Comparison of D/H ratio determinations for solar system objects and the interstellar medium. The shaded area is defined from the 1 σ error bars from this investigation. The IRIS value of D/H is adopted as the best value for Jupiter, and, assuming Jupiter has retained its primordial abundance, as the most representative value of the protosolar nebula. See Table 2 for values of (a) through (s).

TABLE 2

SUMMARY OF OBSERVED RATIOS OF D/H

Determination	Relevant Time Period	D/H ($\times 10^5$)	Reference
Earth			
a) Deep ocean HDO	Solar System Formation	15.8 ± 2	1
Jupiter			
b) Atmospheric CH_3D	Solar System Formation	$2.0^{+1.1}_{-0.8}$ [a]	2
c) Atmospheric CH_3D	Solar System Formation	$3.0^{+1.8}_{-1.2}$ [a]	3
d) Atmospheric CH_3D	Solar System Formation	<1.9 [a]	4
e) Atmospheric CH_3D	Solar System Formation	$3.6^{+1.0}_{-1.4}$ [a]	5
f) Atmospheric HD	Solar System Formation	5.6 ± 1.4	6, 7
g) Atmospheric HD	Solar System Formation	5.1 ± 0.7	8
h) Atmospheric HD	Solar System Formation	1.0–2.6 [a]	9
Saturn			
i) Atmosphere HD	Solar System Formation	5.1 ± 0.7	8
j) Atmospheric CH_3D	Solar System Formation	$2.0^{+2.0}_{-1.0}$	10
k) Atmospheric HD	Solar System Formation	5.5 ± 2.9	11
Uranus			
l) Atmospheric HD	Solar System Formation	3.0 ± 1.2	11
m) Atmospheric HD	Solar System Formation	4.8 ± 1.5	12
Protosolar Nebula			
n) Meteoritic He^3	Solar System Formation	0.8–3	13, 14
o) Solar wind He^3	Solar System Formation	2.5 ± 0.5	15
p) Solar wind He^3	Solar System Formation	$2.0^{+1.5}_{-1.0}$	16
Interstellar Medium			
q) D Lyman lines from *Copernicus*	Now	1.8 ± 0.4	17
r) Summary of D/H observations	Now	1.5 ± 1.0	18
s) Reanalysis of D/H observations	Now	2.25 ± 0.25	18

[a] These Jovian D/H values have been computed or recomputed with C/H = 2.07 × solar (Gautier *et al.* 1982), yielding CH_4/total = 1.75×10^{-3}.

REFERENCES.—(1) Craig 1961. (2) Beer and Taylor 1973. (3) Beer and Taylor 1978. (4) Encrenaz *et al.* 1980. (5) This investigation. (6) Trauger *et al.* 1973. (7) McKellar *et al.* 1976. (8) Trauger *et al.* 1977. (9) Combes and Encrenaz 1979. (10) Fink and Larson 1978. (11) Macy and Smith 1978. (12) Trafton and Ramsey 1980. (13) Black 1971. (14) Black 1972. (15) Geiss and Reeves 1972. (16) Geiss and Bochsler 1979. (17) York and Roberson 1976. (18) Bruston *et al.* 1981.

Kaplan 1980) over the values for the outer solar system and for the protosolar nebula. These terrestrial and meteoritic enhancements are generally considered to be caused by fractionation at low temperatures (Geiss and Reeves 1972; Black 1973; Geiss and Reeves 1981). We are concerned with the D/H ratio of the protosolar nebula, and the fractionated inner solar system objects will not be discussed.

The D/H ratio by number may be derived from the CH_3D abundance

$$\frac{D}{H} = \frac{q_{CH_3D}}{4q_{CH_4}} \frac{1}{f}, \quad (6)$$

where the factor of 4 accounts for the replacement of any one of the four H atoms in CH_4 by one D atom in CH_3D. The deuterium chemical fractionation factor, f,

$$f = [D/H]_{methane}/[D/H]_{hydrogen} \quad (7)$$

is determined by chemical and convective processes in the deep atmosphere of Jupiter. The derivation of the appropriate value of f has been discussed by Beer and Taylor (1973, 1978), and their value of 1.37 has been adopted. Note, however, that Black (1973) has pointed out that the presence of dust in the Jovian atmosphere could increase considerably the value of f.

Owen *et al.* (1979) have demonstrated that dust is entering the Jovian atmosphere from the rings. Prior to the *Voyager* IRIS determination (Gautier *et al.* 1982), a large uncertainty existed in the CH_4 mole fraction. Several recent investigations had indicated the carbon abundance to be enhanced by a factor of 2–5 over the solar value (for a review, see Gautier *et al.* 1982; Wallace and Hunten 1978). Other investigations favor the solar value (Combes and Encrenaz 1979); these authors have recently revised their analysis to 1.9 ± 0.6 times the solar value (Encrenaz and Combes 1982). In the present investigation we have adopted the CH_4 value of Gautier *et al.* (1982), derived from the IRIS experiment, which is 2.07 times solar ($q_{CH_4} = 1.75 \pm 0.2 \times 10^{-3}$). To make the comparisons internally consistent, we have normalized all the Jovian D/H ratios inferred from CH_3D measurements to this same value of q_{CH_4}. The D/H ratio for this investigation is $3.6^{+1.0}_{-1.4} \times 10^{-5}$. In general, fair agreement exists among the four determinations of D/H from atmospheric CH_3D.

Two recent determinations of D/H from CH_3D measurements by Drossart *et al.* (1982) and Knacke *et al.* (1982) are not included in Table 2. Drossart *et al.* (1982) have derived a value of $D/H = 1.8^{+1.4}_{-0.9} \times 10^{-5}$ from *Voyager* IRIS data in the 2200 cm^{-1} region. The Knacke *et al.* (1982) value is $3.8 \pm 0.56 \times 10^{-5}$ after renormalization to the Gautier *et al.* (1982) CH_4 value.

The deuterium abundance of the Jovian atmosphere has also been derived from HD lines. Trauger *et al.* (1973) measured the $P_4(1)$ line of HD, and by comparison with the $S_4(1)$ line of H_2 inferred a D/H value of $2.1 \pm 0.4 \times 10^{-5}$. Based on new laboratory parameters for the $P_4(1)$ HD line, McKellar, Goetz, and Ramsay (1976) have revised the D/H value to $5.6 \pm 1.4 \times 10^{-5}$. New results by Trauger, Roesler, and Mickelson (1977), based on more recent measurements of the $P_4(1)$ HD line, yield $D/H = 5.1 \pm 0.7 \times 10^{-5}$. The Trauger, Roesler, and Mickelson (1977) HD data have also been analyzed by Combes and Encrenaz (1979) by comparison of the HD line strength to that of a weak CH_4 band. Renormalizing to the 2.07 solar C/H value yields $D/H = (1.0\text{–}2.6) \times 10^{-5}$. More recently they have re-estimated their value to $D/H = 1.6^{+1.6}_{-1.0} \times 10^{-5}$ (Encrenaz and Combes 1982). The comparison of the D/H ratios inferred from the CH_3D measurements and the HD analysis of Trauger *et al.* (1973) and Trauger, Roesler, and Mickelson (1977) indicates a systematic difference. The reanalysis of the HD lines by Combes and Encrenaz (1979) eliminates this difference; all methods, including those using meteoritic and solar wind data, seem to be in general agreement.

The D/H ratio has also been determined for Saturn and Uranus by Fink and Larsen (1978), Macy and Smith (1978), and Trafton and Ramsey (1980). The results are in modest agreement with the Jupiter values. As for Jupiter, the determinations from HD are slightly higher than those from CH_3D. Tentative identifications of CH_3D in the atmosphere of Titan have been made by Lutz *et al.* (1981) and Gillett (1975). The two determinations for Uranus, from HD, are also in modest agreement with the Jovian values.

Assuming deuterium was originally homogeneously distributed in the solar nebula, the outer planets may still show variations in D/H due to fractionation during planetary formation as predicted by Hubbard and MacFarlane (1980). However, they find that the value of D/H for Jupiter and for Saturn should both be similar to that of the protosolar nebula, independent of the individual formation processes. Therefore, the value of D/H in this paper should represent the best available value for the solar nebula, due mainly to the relatively unambiguous interpretation of the clear regions in the NEB.

An independent value of the protosolar D/H value can be estimated from He^3 in gas-rich meteorites and in the solar wind. Black (1971, 1972) has estimated $0.8 \times 10^{-5} < D/H < 3 \times 10^{-5}$ for the proto-Sun from He^3 in gas rich meteorites. Geiss and Reeves (1972), and Geiss and Bochsler (1979) obtained $D/H = 2\text{–}2.5 \times 10^{-5}$ from the He^3/H ratio in the solar wind. Our value of $D/H = 3.6^{+1.0}_{-1.4} \times 10^{-5}$ is therefore in reasonable agreement with the value derived from He^3 in gas-rich meteorites and the solar wind. The close agreement implies the absence of fractionation in the solar nebula.

Many measurements of D/H exist for the interstellar medium, with the first identification of interstellar deuterium being in DCN in the Orion molecular cloud (Jefferts, Penzias, and Wilson 1973; Cesarsky, Moffett, and Pasochoff 1973). The D/H values derived from the DCN/HCN ratio and from other deuterated molecules (HD, DCO^+, NH_2D, DC_5N, ...) are difficult to evaluate quantitatively, due to chemical fractionation effects (Solomon and Woolf 1973). The most reliable value of interstellar D/H results from *Copernicus* observations of the deuterium and hydrogen Lyman lines in the line of sight of early-type stars. From observations of five stars, Rogerson and York (1973) and York and Rogerson (1976) have determined $D/H = 1.8 \pm 0.4 \times 10^{-5}$. From observations of ten stars, Laurent, Vidal-Madjar, and York (1979) and Bruston *et al.* (1981) indicate a mean value of $1.5 \pm 1.0 \times 10^{-5}$. Bruston *et al.* (1981) have reanalyzed the interstellar deuterium data, correcting for selective effects due to radiation pressure and UV photodissociation (from shielding of H_2), suggesting an unperturbed $D/H = 2.25 \pm 0.25 \times 10^{-5}$. The interstellar D/H values determined from the Lyman lines exhibit a significant spread, indicating inhomogeneities in the interstellar medium and other uncertainties in the interpretation, such as the number of absorbing clouds along the line of sight. As seen in Figure 19, the interstellar D/H values tend to be slightly lower than those of the outer solar system and the protosolar nebula. This is in accordance with some deuterium depletion from stellar processing since the time of solar system formation.

The big bang is the most viable mechanism for producing deuterium (Epstein, Lattimer, and Schramm 1976), and thus its abundance is of cosmological

significance. The primordial D/H value is a sensitive parameter to the present-day baryon density, which can be used to infer the matter density at the time of the big bang (Wagoner 1973). The amount of deuterium presently observed can easily be produced with standard cosmological models of the big bang (Wagoner 1979; Wagoner 1973; Wagoner, Fowler, and Hoyle 1967). Although other noncosmological mechanisms are capable of producing significant amounts of deuterium, such as shock waves, supernova explosions, etc., none seems plausible or necessary (Epstein, Lattimer, and Schramm 1976). The time evolution of D/H after synthesis in the big bang can be computed with models of chemical evolution in a galaxy. We have presented in Figure 20 two evolutionary abundance curves (EAC) of deuterium from Audouze and Tinsley (1974). As an illustration of the sensitivity of D/H to the assumptions involved in galactic evolution models, two contrasting models are presented, the infall and the no infall model.

The infall model assumes extragalactic gas of primordial big bang composition enters the Galaxy during its evolution at a rate of 2% of the total mass per 10^9 yr. The no infall model does not assume an external flux of gas. In addition the infall model assumes intense star formation during the first 10^9 yr, transforming D rapidly to He^3; the D later is replenished from the primordial D in the infalling gas. The no infall model has a lower, more extended rate of star formation, and the D is gradually destroyed through stellar processing.

Also shown on Figure 20 are the observed D/H values for Jupiter from this investigation and for the protosolar nebula from Geiss and Bochsler (1979), for the time of solar system formation. The EAC curves have been normalized to pass through the center D/H value from this investigation. The observed values for the interstellar medium, corresponding in time to now, are shown from the summary of Bruston *et al.* (1981). Both galactic evolution models give agreement with the solar system formation D/H observations. However, the infall model predicts a higher D/H value than is presently observed and is thus excluded by observations. However, the infall model could be made consistent with observations for both time periods by varying the birthrate function or the rate of infall. Thus the model of galactic evolution introduces some uncertainty in determining the value of primordial big bang D/H from solar system and interstellar medium observations. On the other hand, it should be possible in the future, with smaller uncertainties in the observations, to define better both the value of primordial and interstellar D/H and the models of galactic chemical evolution. Comparisons of the D/H observations to the galactic evolution model of Audouze and Tinsley (1974) which include the production of D in supernova envelopes excludes the supernova mechanism as a significant source of D.

Even with the large uncertainties in the observations and in the models, we can infer information concerning the present-day baryon density. Using the IRIS D/H error bars, we extrapolate back in time to a range in primordial D/H ratio by number of $(5.5\text{–}8.1) \times 10^{-5}$ for the no infall model and $(6.9\text{–}9.0) \times 10^{-5}$ for the infall model. The primordial big bang D/H values have been converted to present-day baryon density using Table 1 of Wagoner (1973); this relationship is

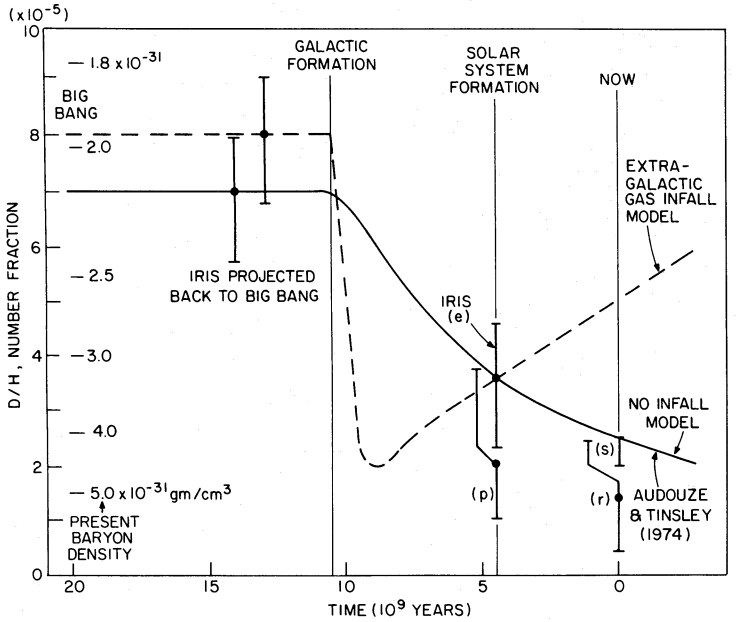

FIG. 20.—Evolutionary abundance curve (EAC) for D/H. The effect of galactic chemical evolution on the D/H ratio is illustrated by two contrasting models of Audouze and Tinsley 1974. The EAC curves have been normalized to pass through the central D/H value from this investigation. The EAC curves have been used to determine the primordial D/H ratio, and subsequently the present-day baryon density. The IRIS determined present-day baryon densities are consistent with an open universe for either of the galactic evolution models.

illustrated on the left of Figure 20. The range of present-day baryon densities is ~ 2.0–2.4×10^{-31} g cm^{-3} for the no infall model and ~ 1.8–2.2×10^{-31} g cm^{-3} for the infall model and is in good agreement with values recently derived by Spite and Spite (1982) from the determination of lithium in stars of Population II. This range represents an upper limit for the present baryon density and leads to an open universe in the standard big-bang models (Wagoner 1973), a critical density of 4.5×10^{-30} g cm^{-3} and of 1.8×10^{-29} g cm^{-3} being required to close the universe for a Hubble expansion parameter H_0 of 50 and of 100 km s^{-1} Mpc^{-1}, respectively (Epstein, Lattimer, and Schramm 1976).

If massive neutrinos dominate the universe, a question which is still open, the production of primordial deuterium would not be changed, in the standard model, and the present derivation of the baryon density is still valid, but the total density could be drastically higher and the universe could be closed.

VIII. CONCLUSIONS

The *Voyager* IRIS measurements offer improvements in composition information over previous ground-based and airborne data because of high spatial resolution, which allows the selection of "cloud-free" regions within the NEB, and because of the wide spectral range, which allows the retrieval of temperature structure and gas composition for the same volume element at the same time. Also, the wide spectral range is more constraining on the altitude distributions of the gases with spectral features occurring in several regions throughout the 180–2250 cm^{-1} range (NH_3, PH_3, and CH_3D), than when only one narrow spectral region needs to be fitted.

An average spectrum representing a very homogeneous "cloud-free" region in the NEB has been constructed from 51 individual *Voyager* IRIS spectra of the clearest regions in the NEB. The average spectrum has been compared to synthetic spectra to derive gas composition information for altitudes corresponding to 0.2–5 bars. Altitude profiles have been derived for NH_3, PH_3, CH_3D, GeH_4, and H_2O. The retrieved profile for NH_3 is close to saturation in the 0.2–0.4 bar range, then follows an increasing subsaturation profile, reaching a depletion factor of ~ 3 at 0.7 bar. In the 0.8–1 bar range, the derived value is $q_{NH_3} = 1.78 \pm 0.89 \times 10^{-4}$, in agreement with the solar value of Lambert (1978). The inferred NH_3 distribution for the NEB is in agreement with the concept of a belt being a down-welling region which is depleted in condensible gases. The PH_3 inferred distribution shows depletion in the 0.4–0.7 bar range. Comparison to the semi-quantitative photochemical models of Strobel (1977) indicates best agreement with the model prediction for coupled NH_3-PH_3 photochemistry. The PH_3 abundance of the 1–4 bar region was $q_{PH_3} = 6 \pm 2 \times 10^{-7}$ which is in agreement with the solar value of Cameron (1973). The mole fraction for CH_3D, determined from the 1120–1220 cm^{-1} and 2100–2200 cm^{-1} spectral ranges, was found to be $q_{CH_3D} = 3.5^{+1.0}_{-1.3} \times 10^{-7}$. The GeH_4 mole fraction of $7 \pm 2 \times 10^{-10}$ at the 2–5 bar level is a factor of 10 lower than the solar value. The H_2O mole fraction is $\sim 1 \times 10^{-6}$ at 2.5 bar increasing to $\sim 3 \times 10^{-5}$ at the 4 bar level. The IRIS inferred distributions for NH_3, PH_3, CH_3D, GeH_4, and H_2O probably represent the best values to date for the NEB, due to the relatively unambiguous interpretation from a homogeneous relatively "cloud-free" region.

The determination of D/H for Jupiter has also been improved through the use of the more accurate values of q_{CH_3D} and q_{CH_4} inferred from the IRIS measurements. Our value of $D/H = 3.6^{+1.0}_{-1.4} \times 10^{-5}$ is in reasonable agreement and consistent with the D/H values derived from He^3 in gas-rich meteorites and the solar wind. If the Jovian atmospheric D/H value is representative of the bulk planet, the agreement with the meteoritic and solar wind values implies that Jupiter has retained its proto-solar nebula value without fractionation during accretion.

The abundance of primordial deuterium formed in the standard big bang model is a sensitive indicator of the present baryon density of the universe. Taking the IRIS value of D/H as representative of the solar nebula at the time of the solar system formation and correcting for the time evolution of D/H with the model for chemical evolution of the galaxy of Audouze and Tinsley (1974), a value of 5.5–9.0×10^{-5} is obtained for the primordial D/H ratio. This ratio yields 1.8–2.4×10^{-31} g cm^{-3} as an upper limit to the present-day baryon density and leads to an open universe in the standard big bang models (Wagoner 1973), provided that the mass of the universe is dominated by baryons.

We wish to thank J. Schneider for a number of enlightening discussions on the big bang theory, and G. Tarrago and G. Poussique for providing us with CH_3D and PH_3 data before publication. We would also like to thank G. Bjoraker for helpful discussions on the 1800–2250 cm^{-1} region analysis and J. Tingley for his contributions in the synthetic modeling. We would like to acknowledge F. and M. Spite for helpful discussions on the lithium problem, and C. Laurent and T. Owen for critically reading the manuscript.

APPENDIX

SUMMARY OF MOLECULAR PARAMETERS

A summary of the important molecular parameters for the strongest absorption bands is given in Table 3.

The determination of the H_2 absorption coefficient is based on the laboratory and theoretical work of Birnbaum and Cohen (1976), Birnbaum (1978), and Cohen and Birnbaum (1981). The absorption lines for the ν_4 bands of $^{12}CH_4$ and $^{13}CH_4$ are from the GEISA spectral line parameter compilation (Chedin *et al.* 1980). Spectroscopic data of the ν_4 band of methane are from Orton and Robiette (1980) and from Toth *et al.* (1981). The $^{12}CH_4$ band intensity is from Chedin *et al.* (1978), the terrestrial ratio of 89 was assumed for the $^{12}CH_4/^{13}CH_4$ ratio. The pressure broadened half-widths were taken as 0.075 and 0.045 cm^{-1} for CH_4-H_2 and CH_4-He collisions, respectively (Varanasi and Tejwani 1972). The absorption lines for CH_3D are from the GEISA line parameters compilation (Chedin *et al.* 1980). The molecular parameters are from Pinkley *et al.* (1977) for the ν_6 CH_3D band, from Tarrago, Rao, and Pinkley (1980) for the ν_3 and the ν_5 band. The ν_6, ν_3, and ν_5 band intensities listed in Table 1 are from G. Tarrago (1980, private communication). The molecular parameters for the ν_2 CH_3D band have been generated using symmetric rotor theory (Allen and Cross 1963; Allen and Plyler 1959). The band intensity for this band is based on the multiplet analysis of lines by Sarangi and Varanasi (1975). The half-widths were assumed to be the same as for CH_4.

The molecular line parameters for the $^{14}NH_3$ and $^{15}NH_3$ bands have been generated by Husson *et al.* (1979) from standard pyramidal XY_3 formulation. The pure rotation transitions in the ground state, and the rotation-inversion transitions in the ν_2 and $2\nu_2$ levels of $^{14}NH_3$ have been reinvestigated by Husson, Goldman, and Orton (1981). The band intensity adopted for the rotational NH_3 band was from Husson, Goldman, and Orton (1982), and for the ν_2 bands from Taylor (1973). The ν_4 band at 1627 cm^{-1} was computed from the work of Curtis (1974) with the band intensity from McKean and Schatz (1956). The $2\nu_2{}^s$ band intensity was normalized to be consistent with the *Voyager* IRIS spectrum for a solar NH_3 mixing ratio of 1.78×10^{-4}. This derived intensity represents a lower limit to the true band intensity. The hydrogen broadened half-width was assumed to be 0.075 cm^{-1} (Varanasi 1972) with the helium broadened value being 0.025 cm^{-1} (Berge and Gulkis 1976).

Spectral line parameters for PH_3 were adopted from Tarrago, Dang-Nhu, and Goldman (1981) for ν_2 and ν_4, from Goldman (1979) for ν_1 and ν_3, and from Goldman (1980) for the 1925–2160 cm^{-1} region. The ν_2, ν_4, ν_1, and ν_3 band intensities are from McKean and Schatz (1956) and the 1925–2160 cm^{-1} band intensity is from Goldman (1980). As no experimental values are available, the PH_3 half-widths were taken to be the same as those of NH_3. The H_2O line parameters are from the ARCRL Atmospheric Line Parameters Compilation (McClatchey *et al.* 1973) with the half-width values from the microwave measurements of the 22 GHz H_2O line (Liebe and Dillon 1969).

The GeH_4 molecular parameters have been generated for the ν_3 band by using spherical top theory for triply-degenerate fundamentals. The rotational constants are from Lepage, Bregier, and Saint-Loup (1976) and the

TABLE 3

SUMMARY OF MOLECULAR DATA FOR STRONGEST ABSORPTION BANDS

Gas	Band Center (cm^{-1})	Band Designation	Band Intensity: 296 K ($cm \cdot molec^{-1}$)	Band Intensity: STP ($cm^{-2}\ atm^{-1}$)	Band Intensity: 300 K ($cm^{-2}\ atm^{-1}$)	α(X-H_2) ($cm^{-1}\ atm^{-1}$)	α(X-He) ($cm^{-1}\ atm^{-1}$)
CH_4	1304	ν_4	5.72×10^{-18}	153.8	140.0	0.075	0.045
CH_3D	1161	ν_6	2.45×10^{-18}	65.9	60.0	0.075	0.045
	1307	ν_3	1.84×10^{-18}	49.4	45.0	0.075	0.045
	1471	ν_5	0.61×10^{-18}	16.5	15.0	0.075	0.045
	2200	ν_2	1.04×10^{-18}	27.9	25.4	0.075	0.045
NH_3	50–250	Rotational	18.1×10^{-18}	486.3	442.8	0.075	0.025
	629	$2\nu_2{}^s - \nu_2{}^a$	1.49×10^{-18}	4.0	3.6	0.075	0.025
	932, 968	ν_2	21.6×10^{-18}	580.9	528.9	0.075	0.025
	950	$2\nu_2{}^a - 2\nu_2{}^s$	0.089×10^{-18}	2.4	2.2	0.075	0.025
	1627	ν_4	4.50×10^{-18}	120.8	110.0	0.075	0.025
	1882	$2\nu_2{}^s$	0.0007×10^{-18}	0.02	0.02	0.075	0.025
PH_3	992	ν_2	3.35×10^{-18}	90.1	82.0	0.075	0.025
	1118	ν_4	4.17×10^{-18}	112.0	102.0	0.075	0.025
	1925–2160	...	0.13×10^{-18}	3.6	3.3	0.075	0.025
	2311	ν_1	10.63×10^{-18}	285.6	260.0	0.075	0.025
	2320	ν_3	10.63×10^{-18}	285.6	260.0	0.075	0.025
H_2O	1595	ν_2	10.6×10^{-18}	285.1	259.6	0.084	0.025
GeH_4	2112	ν_3	45.0×10^{-18}	1208.1	1100	0.075	0.045

band intensity is based on Fink, Larson, and Treffers (1978); the line half-widths are from Corice, Fox, and Fletcher (1972).

The interpretation of the IRIS data is limited in many instances by a lack of knowledge in the basic molecular data. The most significant molecular shortcoming for investigations of the deep atmosphere of Jupiter is the far-wing line shape arising from CH_4-H_2 and NH_3-H_2 collisions which strongly affects interpretation of all Jovian window measurements. The sensitivity of the continuum to the far-wing line shape has been illustrated in this paper for the 1100–1200 window. The effect is even stronger in the 1800–2250 cm^{-1} window. Further advances in interpretation of the deep atmosphere of Jupiter from window measurements are contingent on improved knowledge of the CH_4-H_2 and NH_3-H_2 far-wing line shape.

REFERENCES

Allen, H. C., and Cross, P. C. 1963, *Molecular Vib-rotors* (New York: John Wiley and Sons).
Allen, H. C., Jr., and Plyler, E. K. 1959, *J. Res. NBS*, **63A**, 145.
Atreya, S. K., Donahue, T. M., and Kuhn, W. R. 1977, *Icarus*, **31**, 348.
Audouze, J., and Tinsley, B. M. 1974, *Ap. J.*, **192**, 487.
Baluteau, J. P., Marten, A., Bussoletti, E., Anderegg, M., Moorwood, A. F. M., Beckman, J. E., and Coron, N. 1978, *Astr. Ap.*, **64**, 61.
Baluteau, J. P., Marten, A., Moorwood, A. F. M., Anderegg, M., Biraud, Y., Coron, N., and Gautier, D. 1980, *Astr. Ap.*, **81**, 152.
Barshay, S. S., and Lewis, J. S. 1978, *Icarus*, **33**, 593.
Beer, R., and Taylor, F. W. 1973, *Ap. J.*, **179**, 309.
———. 1978, *Ap. J.*, **219**, 763.
———. 1979, *Icarus*, **40**, 189.
Berge, G. L., and Gulkis, S. 1976, in *Jupiter*, ed. T. Gehrels (Tucson: University of Arizona Press), p. 621.
Birnbaum, G. 1978, *J. Quant. Spectrosc. Rad. Transf.*, **19**, 51.
———. 1979, *J. Quant. Spectrosc. Rad. Transf.*, **21**, 597.
Birnbaum, G., and Cohen, E. R. 1976, *Canadian J. Phys.*, **54**, 593.
Bjoraker, G., Fink, U., Larson, H. P., and Kunde, V. G. 1981, *Bull. AAS*, **13**, 735.
Black, D. C. 1971, *Nature Phys. Sci.*, **234**, 148.
———. 1972, *Geochim. Cosmochim. Acta*, **36**, 347.
———. 1973, *Icarus*, **19**, 154.
Boato, G. 1954, *Geochim. Cosmochim. Acta*, **6**, 209.
Bruston, P., Audouze, J., Vidal-Madjar, A., and Laurent, C. 1981, *Ap. J.*, **243**, 161.
Cameron, A. G. W. 1973, *Space Sci. Rev.*, **15**, 121.
Cesarsky, D. A., Moffett, A. J., and Pasochoff, J. M. 1973, *Ap. J. (Letters)*, **180**, L1.
Chedin, A., Husson, N., Scott, N. A., Cohen-Halluleh, I., and Berroir, A. 1980, Internal Reports 108 and 113, LMD, Ecole Polytechnique, Palaiseau, France.
Chedin, A., Husson, N., Scott, N. A., and Gautier, D. 1978, *J. Molec. Spectrosc.*, **71**, 343.
Cohen, E. R., and Birnbaum, G. 1981, National Bureau of Standards report NBSIR 80-2175(R) (Washington, D.C.: National Bureau of Standards).
Combes, M., and Encrenaz, T. 1979, *Icarus*, **39**, 1.
Combes, M., Courtin, R., Caldwell, J., Encrenaz, T., Fricke, K. H., Moore, V., Owen, T., and Butterworth, P. S. 1981, in *Advances in Space Research. Planetary Aeronomy and Astronomy*, Vol. **1**, No. 9, ed. S. K. Atreya and J. J. Caldwell.
Conrath, B. J., and Gautier, D. 1979, Workshop on Interpretation of Remotely Sensed Data, Williamsburg, Va., May 23–25.
Conrath, B. J., and Revah, I. 1972, Proc. Workshop on Mathematics of Profile Inversion, NASA TM-X-62150.
Corice, R. J., Jr., Fox, K., and Fletcher, W. H. 1972, *J. Mol. Spectrosc.*, **41**, 95.
Craig, H. 1961, *Science*, **133**, 1833.
Curtis, J. 1974, *Dissertation*, Ph.D. thesis, Ohio State University.
Drossart, P., Encrenaz, T., Kunde, V., Hanel, R., and Combes, M. 1982, *Icarus*, in press.
Encrenaz, T., and Combes, M. 1981, in *IAU Symposium 96, Infrared Astronomy*, ed. C. G. Wynn-Williams and D. P. Cruikshank (Dordrecht: Reidel), p. 1.
———. 1982, preprint.
Encrenaz, T., Combes, M., and Zeau, Y. 1978, *Astr. Ap.*, **70**, 19.
Encrenaz, T., Combes, M., and Zeau, Y. 1980, *Astr. Ap.*, **84**, 148.
Epstein, R. I., Lattimer, J. M., and Schramm, D. M. 1976, *Nature*, **263**, 198.
Erickson, E. F., Goorvitch, D., Simpson, J. P., and Stecker, D. W. 1978, *Icarus*, **35**, 61.
Fink, U., and Larson, H. P. 1978, *Science*, **201**, 343.
Fink, U., Larson, H. P., and Treffers, R. R. 1978, *Icarus*, **34**, 344.
Gautier, D., Bezard, B., Marten, A., Baluteau, J. P., Scott, N., Chedin, A., Kunde, V., and Hanel, R. 1982, *Ap. J.*, **257**, 901.
Gautier, D., Conrath, B., Flasar, M., Hanel, R., Kunde, V., Chedin, A., and Scott, N. 1981, *J. Geophys. Res.*, **86**, 8713.
Gautier, D., Lacombe, A., and Revah, I. 1977, *J. Atmos. Sci.*, **34**, 1130.
Gautier, D., Marten, A., Baluteau, J. P., and Lacombe, A. 1979, *Icarus*, **37**, 214.
Geiss, J., and Bochsler, P. 1979, *Proc. 4th Solar Wind Conference, Burghausen* (Berlin: Springer).
Geiss, J., and Reeves, H. 1972, *Astr. Ap.*, **18**, 126.
———. 1981, *Astr. Ap.*, **93**, 189.
Gillett, F. C. 1975, *Ap. J. (Letters)*, **201**, L41.
Goldman, A. 1979, Stratospheric Molecular Parameters Study, University of Denver.
———. 1980, Stratospheric Molecular Parameters Study, University of Denver.
Goorvitch, D., Erickson, E. F., Simpson, J. P., and Tokunaga, A. T. 1979, *Icarus*, **40**, 75.
Hanel, R., *et al.* 1979, *Science*, **204**, 972.
Hubbard, W. B., and MacFarlane, J. J. 1980, *Icarus*, **44**, 676.
Husson, N., Chedin, A., and Scott, N. A. 1979, Internal report 90, LMD, Ecole Polytechnique, Palaiseau, France.
Husson, N., Goldman, A., and Orton, G. 1982, *J. Quant. Spectrosc. Rad. Transf.*, **27**, 505.
Jefferts, K. B., Penzias, A. A., and Wilson, R. W. 1973, *Ap. J. (Letters)*, **179**, L57.
Knacke, R. F., Kim, S. J., Ridgway, S. T., and Tokunaga, A. T. 1982, *Ap. J.*, **262**, 388.
Kolodny, Y., Kerridge, J. F., and Kaplan, I. R. 1980, *Earth Planet. Sci. Letters*, **46**, 149.
Kunde, V. G. 1982, in *Vibrational Rotational Spectroscopy for Planetary Atmospheres*, ed. M. Mumma, K. Fox, and J. Hornstein, NASA Conference Publication 2223.
Kunde, V. G., and Maguire, W. C. 1974, *J. Quant. Spectrosc. Rad. Transf.*, **14**, 803.
Lacy, J. H., Larabee, A. I., Wollman, E. R., Geballe, T. R., Townes, C. H., Bregman, J. D., and Rank, D. M. 1975, *Ap. J. (Letters)*, **198**, L145.
Lambert, D. 1978, *M.N.R.A.S.*, **82**, 249.
Larson, H. P. 1977, Proc. Symposium Planetary Atmospheres, Ottawa, ed. E. V. Jones.
Larson, H. P., Fink, U., Treffers, R., and Gautier, T. N., III. 1975, *Ap. J. (Letters)*, **197**, L137.
Larson, H. P., Treffers, R. R., and Fink, U. 1977, *Ap. J.*, **211**, 972.
Laurent, C., Vidal-Madjar, A., and York, D. G. 1979, *Ap. J.*, **229**, 923.
Lepage, P., Bregier, R., and Saint-Loup, R. 1976, *Compt. Rend. Acad. Sci., Paris, B*, **283**, 179.
Liebe, H. J., and Dillon, T. A. 1969, *J. Chem. Phys.*, **50**, 727.
Lutz, B. L., de Bergh, C., Maillard, J. P., Owen, T., and Brault, J. 1981, *Ap. J. (Letters)*, **248**, L141.

Macy, W., Jr., and Smith, W. H. 1978, *Ap. J.* (*Letters*), **222**, L73.
Marten, A., Courtin, R., Gautier, D., and Lacombe, A. 1980, *Icarus*, **41**, 410.
Marten, A., *et al.* 1981, *Icarus*, **46**, 233.
McClatchey, R. A., Benedict, W. S., Clough, S. A., Burch, D. E., Calfee, R. F., Fox, K., Rothman, L. S., and Garing, J. S. 1973, AFCRL-TR-73-0096.
McKean, D. C., and Schatz, P. N. 1956, *J. Chem. Phys.*, **24**, 316.
McKellar, A. R. W., Goetz, W., and Ramsay, D. A. 1976, *Ap. J.*, **207**, 663.
Orton, G. S., and Robiette, A. G. 1980, *J. Quant. Spectrosc. Rad. Trans.*, **24**, 81.
Owen, T., Danielson, G. E., Cook, A. F., Nausen, C., Hall, V. L., and Duxbury, T. C. 1979, *Nature*, **281**, 442.
Pinkley, L. W., Rao, K. N., Tarrago, G., Poussique, G., and Dang-Nhu, M. 1977, *J. Mol. Spectrosc.*, **68**, 195.
Prinn, R. G., and Lewis, J. S. 1975, *Science*, **190**, 274.
Ridgway, S. T., Larson, H. P., and Fink, U. 1976, in *Jupiter*, ed. T. Gehrels (Tucson: University of Arizona Press), p. 384.
Ridgway, S. T., Wallace, L., and Smith, G. R. 1976, *Ap. J.*, **207**, 1002.
Robert, F., Merlivat, L., and Javoy, M. 1977, *Meteoritics*, **12**, 349.
———. 1978, *Meteoritics*, **13**, 613.
———. 1979, *Nature*, **282**, 785.
Rogerson, J. B., and York, D. G. 1973, *Ap. J.* (*Letters*), **186**, L95.
Sarangi, S., and Varanasi, P. 1975, *J. Quant. Spectrosc. Rad. Transf.*, **15**, 291.
Schramm, D. N., and Wagoner, R. V. 1974, *Physics Today*, **27**, 41.
Scott, N. A. 1973, *J. Quant. Spectrosc. Rad. Transf.*, **14**, 691.
Scott, N. A., and Chedin, A. 1981, *J. Appl. Meteorol.*, **20**, 802.
Smith, W. L. 1970, *Appl. Optics*, **9**, 1993.
Solomon, P. M., and Woolf, N. J. 1973, *Ap. J.* (*Letters*), **180**, L89.
Spite, M., and Spite, F. 1982, *Nature*, in press.
Strobel, D. F. 1977, *Ap. J.* (*Letters*), **214**, L97.
Tarrago, G., Rao, K. N., and Pinkley, L. W. 1980, *J. Mol. Spectrosc.*, **79**, 31.
Tarrago, G., Dang-Nhu, M., and Goldman, A. 1981, *J. Mol. Spectrosc.*, **88**, 311.
Taylor, F. W. 1973, *J. Quant. Spectrosc. Rad. Transf.*, **13**, 1181 (Erratum 1974, *J. Quant. Spectrosc. Rad. Transf.*, **14**, 547).
Terrile, R. J., Capps, R. W., Backman, D. E., Becklin, E. F., Cruikshank, D. P., Berchman, C. A., and Brown, R. H. 1979, *Science*, **204**, 1007.
Tokunaga, A. T., Knacke, R. F., and Ridgway, S. T. 1980, *Icarus*, **44**, 93.
Tokunaga, A. T., Knacke, R. F., Ridgway, S. T., and Wallace, L. 1979, *Ap. J.*, **232**, 603.
Toth, R. A., Brown, L. R., Hunt, R. H., and Rothman, L. S. 1981, *Appl. Optics*, **20**, 932.
Trafton, L., and Ramsay, D. A. 1980, *Icarus*, **41**, 423.
Trauger, J. T., Roesler, F. L., Carleton, N. P., and Traub, W. A. 1973, *Ap. J.* (*Letters*), **184**, L137.
Trauger, J. T., Roesler, F. L., and Mickelson, M. E. 1977, *Bull. AAS*, **9**, 516.
Varanasi, P. 1972, *J. Quant. Spectrosc. Rad. Transf.*, **12**, 1283.
Varanasi, P., and Tejwani, G. D. T. 1972, *J. Quant. Spectrosc. Rad. Transf.*, **12**, 849.
Wagoner, R. V. 1973, *Ap. J.*, **179**, 343.
———. 1979, *Physical Cosmology*, ed. R. Balian, J. Audouze, and D. N. Schramm (New York: North-Holland), p. 395.
Wagoner, R. V., Fowler, W. A., and Hoyle, F. 1967, *Ap. J.*, **148**, 3.
Wallace, L., and Hunten, D. M. 1978, *Rev. Geophys. Space Phys.*, **16**, 289.
Weidenschilling, S. J., and Lewis, J. S. 1973, *Icarus*, **20**, 465.
Winters, B. H., Silverman, S., and Benedict, W. S. 1964, *J. Quant. Spectrosc. Rad. Transf.*, **4**, 527.
York, D. G., and Rogerson, J. B., Jr. 1976, *Ap. J.*, **203**, 378.

J. P. Baluteau, D. Gautier, and A. Marten: Section d'Astrophysique, Observatoire de Paris, 92190 Meudon, France

A. Chedin, N. Husson, and N. Scott: Laboratoire de Meteorologie Dynamique du CNRS, Ecole Polytechnique, Palaiseau, France

R. A. Hanel: Code 690, Laboratory for Extraterrestrial Physics, NASA/Goddard Space Flight Center, Greenbelt, MD 20771

V. G. Kunde and W. C. Maguire: Code 693.2, Laboratory for Extraterrestrial Physics, NASA/Goddard Space Flight Center, Greenbelt, MD 20771